Analysis of atmospheric ammonia over South and East Asia based on the MOZART-4 model and its comparison with satellite and surface observations

Pooja V. Pawar[1*], Sachin D. Ghude[1], Chinmay Jena[1], Andrea Móring[2,7], Mark A. Sutton[2], Santosh Kulkarni[3], Deen Mani Lal[1], Divya Surendran[4], Martin Van Damme[5], Lieven Clarisse[5], Pierre-François Coheur[5], Xuejun Liu[6], Gaurav Govardhan[1,8], Wen Xu[6], Jize Jiang[7], and Tapan Kumar Adhya[9]

[1]Indian Institute of Tropical Meteorology (IITM), Ministry of Earth Sciences, Pune-411008, India
[2]Centre for Ecology & Hydrology (CEH), Edinburgh, EH26 0QB, UK
[3]Centre for Development of Advanced Computing, Pune-411008, India
[4]Indian MeteorologicalDepartment (IMD), Ministry of Earth Sciences, Pune-411005, India
[5]Université libre de Bruxelles (ULB), Spectroscopy, Quantum Chemistry and AtmosphericRemoteSensing (SQUARES), Brussels, B-1050, Belgium
[6]College of Resources and Environmental Sciences, National Academy of Agriculture Green Development, China Agricultural University, Beijing 100193, China
[7]The University of Edinburgh, Scotland, EH8 9AB, UK
[8]National Centre for Medium Range Weather Forecasting, Noida, Uttar Pradesh, India
[9]Kalinga Institute of IndustrialTechnology, Bhubaneshwar, 751016, India

Correspondence to: Sachin D. Ghude (sachinghude@tropmet.res.in)

Abstract. Limited availability of atmospheric ammonia (NH_3) observations, limits our understanding of controls on its spatial and temporal variability and its interactions with ecosystems. Here we used the Model for Ozone and Related chemical Tracers (MOZART-4) global chemistry transport model and the Hemispheric Transport of Air Pollution version-2 (HTAP-v2) emission inventory to simulate global NH_3 distribution for the year 2010. We presented a first comparison of the model with monthly averaged satellite distributions and limited ground-based observations available across South Asia. The MOZART-4 simulations over South Asia and East Asia were evaluated with the NH_3 retrievals obtained from the Infrared Atmospheric Sounding Interferometer (IASI) satellite and 69 ground based monitoring stations for air quality across South Asia, and 32 ground based monitoring stations from the Nationwide Nitrogen Deposition Monitoring Network (NNDMN) of China. We identified the northern region of India (Indo-Gangetic Plain, IGP) as a hotspot for NH_3 in Asia, both using the model and satellite observations. In general, a close agreement was found between yearly-averaged NH_3 total columns simulated by the model and IASI satellite measurements over the IGP, South Asia ($r = 0.81$) and North China Plain (NCP), of East Asia ($r = 0.90$). However, the MOZART-4 simulated NH_3 column was substantially higher over South Asia than East Asia, as compared with the IASI retrievals, which show smaller differences. Model simulated surface NH_3 concentrations indicated smaller concentrations in all seasons than surface NH_3 measured by the ground based observations over South and East Asia, although uncertainties remain in the available surface NH_3 measurements. Overall, the comparison of East Asia and South Asia using both MOZART-4 model and satellite observations showed smaller NH_3 columns in East Asia compared with South Asia for comparable emissions, indicating rapid dissipation of NH_3 due to secondary aerosol formation, which can be explained by larger emissions of acidic precursor gases in East Asia.

1. Introduction

Gaseous pollution due to various forms of nitrogen emissions plays an important role in environmental processes. Specifically, ammonia (NH_3) emitted from various agricultural activities, such as use of synthetic fertilizers, animal farming, etc., together with nitrogen oxides (NOx) is one of the largest sources of reactive nitrogen (Nr) emission to the atmosphere. Ammonia has great environmental implications due to its substantial influence on the global nitrogen cycle and associated air pollution, ecosystem and on public health (Behera et al., 2013; Liu et al., 2017b; Zhou et al., 2016). Emission estimates provided by latest EDGAR v4.3.2 emission inventory suggests that globally about 59 Tg of NH_3 was emitted in the atmosphere in 2012 out of which direct soil emissions contributed about 56 %, manure management (on farm) contributed about 19 %, and agricultural burning contributed about 1.5 % while biomass burning contribution is not included in emission estimate. Furthermore, due to lack of observed emission factors and high uncertainty of agricultural statistics, the uncertainty of NH_3 is the largest among all other pollutants in EDGAR v4.3.2 (Crippa et al., 2018).Ammonia is a key precursor in aerosol formation, as the reactions in the atmosphere lead to an increase in different forms of sulphates and nitrates that contribute in secondary aerosol formation (Pinder et al., 2007, 2008). India and China together accounted for an estimated 64 % of the total amount of NH_3 emissions in Southern Asia during 2000-2014 (Xu et al., 2018).Emissions of NO_x and NH_3 are increasing substantially over South Asia (Sutton et al., 2017b, 2017a), which contributes to increase in particulate mass loading, visibility degradation, acidification and eutrophication (Behera et al., 2013; Ghude et al., 2008, 2013, 2016). Asia is responsible for the largest share of global NH_3 emissions (Janssens-Maenhout et al., 2012). Further increase in NH_3 emission will increase its negative impacts and societal cost (Sutton et al., 2017b).

In India, around 50 % of total NH_3 emissions is estimated from the fertilizer application and remaining from livestock and other NH_3 sources (Aneja et al., 2011; Behera et al., 2013). However, there are large uncertainties in emissions of ammonia, its deposition to surface, chemistry and transport (Sutton et al., 2013; Zhu et al., 2015). Urea is mostly used as a fertilizer (Fertlizer Association of India annual report 2018-19) and alone contributes more than 90% of total fertilizer used for the agricultural activities (Sharma et al., 2008). India is currently the second largest consumer of fertilizers after China, and fertilizer usage is bound to increase with further intensification of agriculture and the fertilizer input of India is expected to be doubled by 2050 (Alexandratos and Bruinsma, 2012).

Recent study based on Infrared Atmospheric Sounding Interferometer (IASI) satellite measurements show very high concentration of NH_3 over Indo-Gangetic Plain (IGP) and North China Plain (NCP) which were mainly related to agricultural (Van Damme et al., 2014a, 2014b, 2015b)and industrial activity (Clarisse et al., 2019; Van Damme et al., 2018). The seasonality was shown to be more pronounced in the northern hemisphere, with peak columns in spring and summer season (Van Damme et al., 2014a). Van Damme et al., (2015a)attempted first to validate IASI-NH_3 measurements using existing independent ground-based and airborne data sets. This study doesn't include comparison of ground-based NH_3 data sets with IASI measurements particularly over South Asia (India) due to limited availability of NH_3 measurements. Liu et al. (2017a)estimated the ground-based NH_3 concentrations over East Asia, combining IASI-NH_3 columns and NH_3 profiles from MOZART-4 and validated it with forty four sites of Chinese Nationwide Nitrogen Deposition Monitoring Network (NNDMN). In one of the recent study over South Asia, interannual variability of atmospheric NH_3 using IASI observations revealed large seasonal variability in atmospheric NH_3 concentrations

which were equivalent with highest number of urea fertilizer plants. This study highlights the importance of role of agriculture statistics and fertilizer consumption/application in determining ammonia concentration in South Asia (Kuttippurath et al., 2020). Available global ammonia emission inventory does not include a comprehensive bottom up NH_3 emissions for South Asia compared to East Asia to be suitable for input to atmospheric models by taking into consideration actual statistical data of various NH_3 sources such as livestock excreta, fertilizer application, agricultural soil, nitrogen-fixing plants, crop residue compost, biomass burning, urine from rural populations, chemical industry, waste disposal, traffic, etc which is currently missing (Behera et al., 2013; Huang et al., 2012; Janssens-Maenhout et al., 2015; Li et al., 2017; Zhang et al., 2010). Han et al. (2020) suggested that updated emission inventory as per the source activity is essential for south Asia to reduce the uncertainties simulated NH_3 over this region. A recent study by Wang et al. (2020) examined the NH_3 column observed over the IGP during summer using regional model driven with MIX emission inventory. The study suggested that large agriculture activity and high summer temperature contributes to high NH_3 emission fluxes over IGP which leads to large total columns. Summer time increase in NH_3concentration at surface over certain sites in the IGP regions are also observed from the ground based monitoring network (Datta et al., 2012; Mandal et al., 2013; Saraswati et al., 2019; Sharma et al., 2012, 2014b).

In this study, we examined the spatio-temporal variability of atmospheric NH_3 over Asia (South and East Asia) and focus on two hotspots regions of ammonia, the Indo-Gangetic Plain (IGP) and the North China Plain (NCP). The approach for this study is a combination of simulations using chemical transport modelling, satellite observations and *in-situ* ammonia measurements over South Asia (69 stations) and East Asia (32 stations). The analysis applies the Model for Ozone and Related chemical tracers (MOZART-4) driven by priori ammonia emissions based on Hemispheric Transport of Air Pollution version-2 (HTAP-v2) emission inventory. It applies HTAP-v2 data for emissions to produce estimated total columns of NH_3 and aerosol species for the year 2010 over Asia. Model simulations were evaluated and compared with NH_3 data from IASI (over South and East Asia) and selected ground-based observations (noted above). In addition to the regional comparison, we examine why certain emission hotspot regions in East Asia show lower NH_3 total columns compared with similar hotspot regions in South Asia, when analyzed with both model and satellite observations.

2. Data and methodology

2.1 MOZART-4 model

The global chemical transport model MOZART-4 has been employed in this study to conduct a year-long (2010) simulation of atmospheric trace gases and aerosols over Asia using the updated HTAP-v2 emission inventory (Janssens-Maenhout et al., 2015). These simulations were earlier performed to meet the objectives of Task Force on Hemispheric Transport of Air Pollution, phase 2, multi-model experiments (Surendran et al., 2015; Surendran et al., 2016). The model domain covers entire globe at a horizontal grid resolution of 1.9° × 2.5° and 56 vertical levels from the surface upto 1hectopascal (hPa). The model has approximately 10 levels in the boundary layer (below 850 hPa). MOZART-4 takes into account surface emissions, convection, advection, boundary layer transport, photochemistry, and wet and dry deposition. The model simulations were driven by the input meteorological data set of 1.9° × 2.5° resolution from Modern Era Retrospective-analysis for Research (MERRA) and Applications of the Goddard Earth Observing System Data Assimilation System (GEOS-DAS).

Model simulations were performed for the complete year of 2010 (1 January 2010 to 31 December 2010) and its outputs were saved every 6h (4 time steps each day) with a spin up time of six months (1 July 2009 to 31 December 2009). MOZART-4 includes 157 gas-phase reactions, 85 gas-phase species, 39 photolysis and 12 bulk aerosol compounds (Emmons et al., 2010). Dry deposition of gases and aerosols were calculated online according to the parameterization of Wesely (1989) and wet deposition of soluble gases were calculated as described by the method of Emmons et al. (2010). Land use cover (LUC) maps used in MOZART-4 are based on the Advanced Very High Resolution Radiometer (AVHRR) and Moderate Resolution Imaging Spectroradiometer (MODIS) data based on NCAR Community Land Model (CLM) (Oleson et al., 2010). MOZART-4 represents the land surface as a hierarchy of sub-grid types: glacier, lake, wetland, urban and vegetated land. The vegetated land is further divided into a mosaic of Plant Function Type (PFTs). These same maps are used for the dry deposition calculations (Emmons et al., 2010; Oleson et al., 2010; Lawrence and Chase, 2007).In MOZART-4 the tropospheric aerosol component is built on the extended work of Tie et al. (2001 and 2005). Online fast Tropospheric Ultraviolet Visible (FTUV) scheme, based on the TUV model (Tie et al., 2003) is used for the calculation of photolysis rates in MOZART-4. For long-lived species like CH_4 and H_2, surface boundary conditions are constrained by observations from NOAA/ESRL/GMD (Dlugokencky et al., 2005, 2008; Novelli et al., 1999) and as per Intergovernmental Panel N_2O concentrations are set to the value as described in Intergovernmental Panel on Climate Change 2000 report (IPCC, 2000). Biogenic emissions of isoprene and monoterpenes are calculated online using the Model of Emissions of Gases and Aerosols from Nature (MEGAN) (Guenther et al., 2006), using the implementation described by Pfister et al. (2008). Surface moisture flux and all relevant physical parameters are used to calculate water vapor (H_2O) online. Biomass burning emissions of a wide range of gaseous components, including NH_3, SO_2 and individual volatile organic compounds were provided from the Global Fire Emission Database (GFED-v3), determined by scaling the GFED CO_2 emissions by the emission factors provided on 1.9° × 2.5° grid resolution (Emmons et al., 2010).

In MOZART-4 the ammonium nitrate distribution is determined from NH_3 emissions and the parameterization of gas/aerosol partitioning using equilibrium simplified aerosol model (EQSAM) by Metzger et al. (2002), which is a set of approximations to the equilibrium constant calculation (Seinfeld et al., 1998), based on the level of sulphate present. In Metzger et al. (2002) cations other than NH_4^+, e.g., sodium (Na^+), potassium (K^+), calcium (Ca^{2+}), and magnesium (Mg^{2+}) as well as organic acids have been neglected for the gas-aerosol partitioning calculations. Metzger et al. (2006) found that the NH_3/NH_4^+ (calculated by account for ammonium-sulfate-nitrate-sodium-chloride-water system (updated-EQSAM2 parameterization considering organic acids) was 15 % lower than that calculated from the parameterization similar to EQSAM. Ammonia has stronger affinity towards neutralization of sulphuric acid (H_2SO_4) than nitric acid (HNO_3) whereas formation of ammonium chloride (NH_4Cl(s) or (aq)) in atmosphere is unstable and can dissociate reversibly to NH_3 and HCL. These aerosols in both dry and aqueous phase evaporate faster than the corresponding ammonium nitrate (NH_4NO_3) aerosols (Seinfeld and Pandis, 2012). In current modelling setup NH_3/NH_4^+ partitioning is mainly controlled by sulfate and subsequently by nitrate. Recent study (Acharja et al., 2020) based on analysis of water soluble inorganic chemical ions of PM_1, $PM_{2.5}$ and atmospheric trace gases over IGP revealed that NH_4^+ was one of the dominant ions, collectively with Cl^-, NO_3^- and SO_4^- constituted more than 95 % of the measured ionic mass in both PM_1 and $PM_{2.5}$. Remaining ionic species (i.e., Na^+, K^+, Ca^{2+} and Mg^{2+}) formed constituted only about 3% of the total measured ions. Although major mineral cations (i.e., Na^+, K^+, Ca^{2+} and Mg^{2+}) contribute

actively in neutralization reaction, but their concentration in IGP was found to be very low. Also over NCP, mineral cations contributed less than 5 % in both PM_1 and $PM_{2.5}$ (Dao et al., 2014). Furthermore, recent study by Xu et al. (2017) over East Asia revealed that NH_4^+ was the predominant neutralizing cation with the highest neutralization factor (NF) (above 1), whereas Na^+, K^+, Ca^{2+} and Mg^{2+} contributed relatively low (below 0.2). Therefore, consideration of mineral cations and organic acids on the NH_3/NH_4^+ partitioning might be limited and will not have significant impact on the results of this study.

2.2 Emission inventory (HTAP-v2)

The HTAP-v2 bottom-up database is used in this study as an input for anthropogenic emissions of NH_3 for the year 2010 (Janssens-Maenhout et al., 2015). HTAP-v2 dataset is embedded with the activity data as per harmonized emission factors, international standards, and gridded emissions with global proxy data. It includes important point sources providing high spatial resolution and emission grid maps with global coverage. This dataset consists of monthly mean NH_3 emission maps with $0.1^\circ \times 0.1^\circ$ grid resolution for the year 2010. The HTAP-v2 dataset is compiled using various regional gridded emission inventories by Environmental Protection Agency (EPA) for USA and Environment Canada for Canada, European Monitoring Evaluation Programme (EMEP) and Netherlands Organisation for Applied Scientific Research for Europe, and Model Inter comparison Study in Asia (MICS Asia) for China, India and other Asian countries. The emissions Database for Global Atmospheric Research (EDGARv4.3) is used for the rest of the world (mainly South-America, Africa, Russia and Oceania). The 'MICS Asia' dataset incorporated into the HTAP-v2 dataset includes an anthropogenic emission inventory developed in 2010 (Li et al., 2015), which incorporates several local emission inventories, including the Multi-resolution Emission Inventory for China (MEIC), NH_3 emission inventory from Peking University (Huang et al., 2012) and Regional Emission inventory in Asia version 2.1 (REAS2.1) (Kurokawa et al., 2013) for areas where local emission data are not available. A detailed description on HTAP-v2 datasets can be found in Janssens-Maenhout et al. (2015).

For this study, we used emissions from five important sectors, such as, agricultural, residential (heating/cooling of buildings and equipment/lighting of buildings and waste treatment), energy (power industry), transport (ground transport) and industries (manufacturing, mining, metal, cement, chemical, solvent industry) for the year 2010. The aircraft and international shipping is not considered for NH_3 emissions in the HTAP-v2 bottom-up database. These emissions also includes natural emissions such as soil from the Community Earth System Model (CESM), and biomass burning from the Global Fire Emission Database (GFED-v3) (Randerson et al., 2013).All these emissions are re-gridded to $1.9^\circ \times 2.5^\circ$ to match the model resolution.

The spatial distribution of the total NH_3 emissions over Asian region is shown in Fig. 1. It shows the highest emissions over both South and East Asia, especially over the IGP and NCP region (shown with black box in Fig. 1). Agricultural sector is the main contributor to NH_3 emission, including management of manure and agricultural soils (application of nitrogen fertilizers, including animal waste). It also includes emissions from livestock, crop cultivation excluding emissions from agricultural waste burning and savannah burning (Janssens-Maenhout et al., 2015). Minor contributions from the residential sector are also observed for the Asian countries due to use of biomass combustion and coal burning which is also included in the emissions. Spatial proxies such as population density, road networks, and land use information have been used to allocate area of emission sources. For the REAS2 emission inventory over India, the agricultural sector follows spatial proxy of total

population (Li et al., 2017). The use of this approach is expected to be the main source of spatial uncertainty in the estimated NH_3 emissions to the extent that total human population is only approximately correlated with spatial distribution of fertilizer use and livestock numbers. Seasonal variation of average NH_3 emission over the IGP and NCP region for Anthropogenic (HTAP-v2), biomass burning (GFED-v3) and Soil emission (CESM) is shown in Fig. 2. Anthropogenic NH_3 emissions do not show any strong seasonal variability over the IGP region however over the NCP region, NH_3 emissions show strong seasonality with peak emissions between May-September months. It can be seen that the magnitude of peak emissions is two times more over the NCP region than IGP region. On the other hand, seasonality in biomass burning NH_3 emissions is strong over the IGP region, which shows highest emissions in the spring season (MAM). Also, contribution of NH_3 emissions from the IGP region is significantly higher compared to NCP region during peak burning season, but the magnitude of biomass burning emission is six times lower compared to the magnitude of anthropogenic emissions.

2.3 Satellite NH_3 observations

The NH_3 total columns data used in study are derived from the IASI space-borne remote sensing instrument on board Metop-A, which was launched in 2006 in a polar sun-synchronous orbit. The IASI operates in the thermal infrared spectral range (645–2760 cm^{-1}) with mean local solar overpass time of 9:30 am and 9:30 pm (Clerbaux et al., 2009). It covers the globe twice a day with and each observation is composed of 4 pixels with a circular footprint of 12 Kilometer (km) diameter at nadir and elliptical at the end of the swath (20 × 39 km). IASI is a suitable tool for evaluation of regional and global models due to its relatively high spatial and temporal sampling and retrieval algorithms have been continuously improved (Whitburn et al., 2016). The NH_3 total column retrievals show satisfactory agreement with monthly averaged integrated ground-based measurements with FTIR column data (Van Damme et al., 2015a). IASI measurements are also found to be consistent with other NH_3 satellite products (Clarisse et al., 2010; Someya et al., 2020; Viatte et al., 2020). In present study, we have used ANNI-NH_3-v2.2R-I dataset for the year 2010 which relies on ERA-Interim ECMWF meteorological input data, along with surface temperature retrieved from a dedicated network (Van Damme et al., 2017). An improved retrieval scheme for IASI spectra relies on the calculation of a dimensionless "Hyperspectral Range Index," which is successively converted to the total column and allow a better identification of weak point sources of atmospheric NH_3(Van Damme et al., 2017; Whitburn et al., 2016). More details about IASI satellite and NH_3 data product is given in Clerbaux et al. (2009), Van Damme et al. (2017) and Whitburn et al. (2016).We have considered the daily NH_3 cloud-free satellite total column data and compared with the modelled daily NH_3 total column averaging paired observations across the months, seasons and year. We have used only morning overpasses at 9:30 am measurements, as the relative errors due to the lower thermal contrast are larger for the night-time measurements (9:30 pm overpass). For consistency with satellite retrievals, first the model output (11:30 LT) at each day close to satellite overpass time (9:30 LT) is interpolated in space to the location of valid satellite retrievals. Since IASI retrieval algorithm only provides total columns, in second step, we made unweighted average distribution of the daily paired data to obtain a monthly, seasonal and annual mean value of satellite and model total NH_3 columns at each horizontal resolution of the model (1.9° × 2.5°).

2.4 Ground based observations

To evaluate model performance in South Asia, we used hourly NH_3 measurements from the air quality monitoring station (AQMS) network operated by Central Pollution Control Board (CPCB) across India. CPCB follows a national program for sampling of ambient air quality as well as weather parameters measurements. An automatic analyzer (continuous) method is adopted at each monitoring location. NH_3 is measured by the chemiluminescence method as NO_x following oxidation of NH_3 to NO_x. In this approach, NH_3 is determined from the difference between NO_x concentration with and without inclusion of NH_3 oxidation (CPCB, 2011). The quality assurance and control process followed for these air quality monitoring instruments is given in CPCB (2014, 2020).Surface observations of NH_3 are taken from 69 different stations in South Asia. Most of the NH_3 monitoring stations from India used in the current study are situated in the cities representing the urban environment. Sampling of ambient NH_3 is done through a sampling inlet of 1 meter (m) above the roof top of container AQMS having height of 2.5 m (Technical specifications, 2019). The details of these monitoring locations are given in Table S1 (in the Supplement) and the geographical locations are shown in Fig. 3. Out of these stations thirty five locations in Delhi, six in Bangalore city, four in Hyderabad, and two in Jaipur city are averaged to get single value for the same geographical location and the remaining 22 locations are considered independently representing 26 respective cities. Hourly NH_3 concentrations (in $\mu g\ m^{-3}$) used in the study are for the duration of 2016 to 2019. The quality control and assurance method, followed by Central Pollution Control Board (CPCB) for these air quality monitoring stations, is given in the CPCB (2011 and 2020). The calibration procedures for NH_3 analyzer conforms to United States Environmental Protection Agency (USEPA) methodologies and include daily calibration checks, biweekly precision checks and linearity checks every six weeks. All analyzers undergo full calibration every six weeks. For detail on calibration procedure refer to Technical Specifications for Continuous Real Time Ambient Air Quality Monitoring Analysers (2016) and CPCB (2020). Furthermore, we take the following steps to reassure the quality of NH_3 observations from the CPCB network stations. For data quality, we rejected all the observations values below the lowest detection limit of the instrument (1 $\mu g\ m^{-3}$) (Technical specifications for CAAQM station, 2019) because most of the sites are situated in the urban environment. For cities where more than one monitoring station is available, we rejected all the observations above 250 $\mu g\ m^{-3}$ at a given site if other sites in the network do not show values outside this range. This step aims to eliminate any short-term local influence that cannot be captured in the models and retain the regional-scale variability. Second, we removed single peaks characterized by a change of more than 100 $\mu g\ m^{-3}$ in just one hour for all the data in CPCB monitoring stations. This step filters random fluctuations in the observations. Third, we removed some very high NH_3 values that appeared in the time series right after the missing values. For any given day, we removed the sites from the consideration that either experience instrument malfunction, or appear to be very heavily influenced by strong local sources. In order to verify the data quality of CBCB monitoring site, we have inter compared the NH_3measurement at CPCB monitoring station (R.K. Puram) in Delhi with the NH_3 measurements at Indira Gandhi International (IGI) Airport taken during Winter Fog Experiment (WiFEX) (Ghude et al., 2017) using Measurement of Aerosols and Gases (MARGA) instrument during winter season of 2017-2018. More details on the NH_3 measurements using MARGA is available with Acharja et al.(2020). Both sites were situated in the same area of Delhi (less than 1km). Our inter-comparison show that NH_3 measured at CPCB monitoring station by chemiluminescence method are slightly (on an average 9.8 μgm^{-3}) on higher side than NH_3 measured by ion chromatography (IC)

using MARGA (Fig. S1 in the Supplement).The differences that were observed could partly be related to the different NH_3 measurement techniques and partly to the locations of the two monitoring sites which were not place exactly at same location. Apparently, the difference of 9.8 µg m^{-3} indicates that the NH_3 measurements from the CPCB do not suffer from the calibration issue. However, rigorous validation is required in the future with more data sets. Given the presence of relatively high NOx concentrations, especially at urban locations, it is recognized that the measurement of NH_3 by difference (i.e., between NO_x and NO_x plus oxidized NH_3), is a potentially significant source of uncertainty. Future measurement inter-comparisons are planned (rescheduled from 2020 to 2021 because of COVID-19) to allow the chemiluminescence method as used in the Indian network to be compared with a range of other NH_3 measurement methods (Móring et al., 2021; The Global Challenges Research Fund (GCRF) South Asia Nitrogen hub).

To further evaluate model performance over East Asia, we used monthly mean NH_3 measurements from the 32 stations of the Nationwide Nitrogen Deposition Monitoring Network (NNDMN) of China, operated by China Agricultural University. The details of these monitoring locations are given in Table S2 (in the Supplement) and the geographical locations are shown in Fig. 3. Monthly mean NH_3 concentrations (in µg m^{-3}) used in the study are for the duration of 2010 to 2015. Ambient concentrations of gaseous NH_3 were measured using an active Denuder for Long-Term Atmospheric sampling (DELTA) system. More detail about the data product is given by Xu et al. (2019). To compare the model with observation, simulated NH_3 from the model are compared with the surface-based observations by using bi-linear interpolation of model output to the geographical location and elevation of the observational sites.

3. Results and Discussion

3.1 Annual mean NH_3 total columns over South Asia

Yearly-averaged 2010 distribution of NH_3 total columns over Asia simulated by MOZART-4 model and also retrieved with IASI instrument are shown in Fig. 4a and 4b. The total NH_3 columns simulated by the model show high Tropospheric Vertical Column Densities (TVCDs) of about 0.5-7×10^{16} molecules cm^{-2} over IGP region of India compared to any other regions of Asia. This may reflect the larger range of NH_3 column values for the South Asian model domain, with both more polluted and cleaner conditions. These high TVCDs values coincide with the high fertilizer-N and livestock numbers, as scaled according to human population density in Fig. 1.

Spatial differences between model simulated data and satellite data for NH_3 total column distribution are shown in Fig. 4c. On a quantitative level, the MOZART-4 model is found to overestimates the NH_3 total column compared with IASI by 1-4×10^{16} molecules cm^{-2} over South Asia, especially over northeast India and Bangladesh. Conversely, the MOZART-4 model underestimates NH_3 in comparison with IASI over the arid region of north western India (state of Rajasthan adjacent to Pakistan) and centering on Pakistan. There are several possible reasons for the spatial differences shown in Fig. 4c, including: a) uncertainties in the mapped NH_3 emissions data (e.g., between Afghanistan, Bangladesh, India and Pakistan, due to different relationships between human population and livestock/fertilizer activities); b) uncertainties related to turbulent mixing and dispersion (this may affect both the simulations in MOZART-4 and the assumed vertical profiles for the IASI

retrievals); and c) uncertainties related to precipitation scavenging of ammonia and ammonium, noting that the eastern part of the IGP is substantially wetter than the western part.

According to Fig. 1, the magnitude of NH_3 emissions over NCP is similar to IGP. By contrast, much smaller TVCDs of the NH_3 columns are estimated by MOZART-4 and IASI over NCP compared with IGP. The MOZART-4 and IASI estimates are found to be in close agreement, with slightly smaller values estimated by MOZART-4. The possible reasons for the difference in NH_3 concentrations in IGP and NCP are discussed in Sect. 3.4. The relationship between modelled and IASI retrieved NH_3 total columns are further analysed in terms of scatter plots in Fig. 5a and 5b, over IGP region of South Asia (20°N-32°N, 70°E-95°E) and NCP region of East Asia (30°N-40°N, 110°E-120°E) (rectangular areas shown in Fig. 1). Correlation coefficients (r) between model and satellite observed annual mean total columns over IGP and NCP are found to be 0.81 and 0.90 respectively for 2010. This indicates that spatial variability in simulated NH_3 by the model and satellite observation is in closer agreement, both over IGP and NCP region. The Model simulated annual mean total NH_3 columns gives larger values over IGP region (Normalised Mean Bias (NMB) = 38 %) as well as over entire South Asia (NMB = 44 %). Whereas over the NCP region (NMB = -35 %) and entire East Asia (NMB = -32 %), the model gives values which are smaller than IASI. Other statistical indicators are summarised in Table 1. Larger estimates of NH_3 columns from an atmospheric Chemistry Transport Model (CTM) compared with IASI was also found in an earlier study for South Asia (Clarisse et al., 2009).

The overall higher value of the model simulated NH_3 over South Asia compared with IASI could be due to the combination of the uncertainties in both approaches. This includes uncertainties in emissions from the HTAP-v2 datasets used for the model simulations, inaccurate modelling of the chemistry in MOZART-4, errors in dry and wet deposition schemes used in the model, and biases inherent to infrared satellite remote sensing. For IASI, firstly, only cloud-free satellite scenes are processed, which could result in missing partly some of the NH_3 values during cloudy periods and biomass burning events. Secondly, NH_3 vertical columns retrieved from the IASI observations are actually sampled around 9:30 local time while the MOZART-4 simulated model output close to overpass time (11:30 LTC) was used. Finally, the retrieval of NH_3 from infrared satellites is sensitive to inaccuracies in the temperature profile, and biases in the IASI L2 temperature profiles can result in biases in the retrieved NH_3 (Whitburn et al., 2016). The HTAP-v2 dataset use proxy values for agricultural activities (i.e., distributed by human population) instead of actual values for field fertilizer application and livestock excretion over the South Asia. This could also result in additional uncertainty of NH_3 emissions from the agricultural activities. Further work is on-going to integrate NH_3 emissions inventories for different countries in South Asia based on national datasets, which should allow the emissions related uncertainties to be reduced in future. Similarly, slight underestimation over East Asia might originates from the country specific emission inventory used for China (Huang et al., 2012) in MOSAIC HTAP-v2 emission inventory and the limitations discussed above. The application of any equilibrium models (EQMs) in global atmospheric studies is associated with considerable uncertainties. In MOZART-4 chemistry, the ammonium nitrate distribution is determined from NH_3 emissions and the parameterization of gas/aerosol partitioning by Metzger et al. (2002), based on the level of sulphate present. The emission fluxes of SO_2 and NO_X in HTAP-v2 data set also has large uncertainties over the IGP (Jena et al., 2015b; Wang et al., 2020), which can introduce additional uncertainty in NH_3/NH_4^+ gas/aerosol partitioning. In MOZART-4 chemistry, uncertainty can be also associated in dry and wet deposition scheme which can result in overestimation (Emmons et al., 2010).

3.2 Seasonal variability of NH_3 total columns

Figure 6 shows the model (left) and IASI satellite (middle) seasonal distributions of NH_3 total columns over Asia. These seasons are represented as 3-month periods: Winter, December-January-February (DJF, first row), Spring, March-April-May (MAM, second row), Summer, June-July-August (JJA, third row), and Autumn, September-October-November (SON, fourth row). It can be seen in Fig. 6, that there is larger seasonal variation in IASI NH_3 total columns while MOZART-4 presents limited seasonality as in South Asia compare to better seasonal variation estimated in East Asia, as shown by both IASI and the MOZART-4 model. In general, during autumn, spring, summer and winter seasons MOZART-4 shows higher NH_3 total column compared with IASI estimates over most of South Asia. However, this difference is more pronounced during autumn (SON) and winter (DJF) seasons (Fig. 6; Right). We have seen that (Fig. 2) anthropogenic emission of NH_3 is nearly same in all months and biomass burning has peak during MAM over South Asia in the MOZART-4 model. Whereas, seasonality is better represented in NH_3 emission for East Asia.

Major drivers in anthropogenic NH_3 seasonal variation include differences in management and timing of fertilizer, which is not well represented in the emission over South Asia (Janssens-Maenhout et al., 2012). This can be expected to have the direct effect on NH_3 total column over South Asia. It is recognized that NH_3 emission can be strongly affected by both short term meteorological variation and longer term climatic differences (Sutton et al., 2013). This means that NH_3 emissions may be expected to increase in warm summer conditions than in winter (Battye and Barrows, 2004). However, magnitude of these emissions is expected to be smaller in comparison with anthropogenic emissions and may not contribute significantly to larger summertime NH_3 columns observed from IASI retrievals over South Asia and East Asia than MOZART-4. Additional driver in NH_3 seasonal variation include meteorological variation. For example, strong subsidence, lower temperature and lighter winds over South Asia in the autumn and winter months prevent venting of low altitude pollution to the higher altitudes. This means that emitted air pollutants tend to accumulate close to the source region in winter time conditions (Ghude et al., 2010, 2011). Considering the comparison of IGP with NCP, accumulation of pollutants in the boundary layer is more pronounced over IGP region due to flat land topography, and it is more during winter than the autumn months (Surendran et al., 2016). We saw that simulated mean Planetary boundary layer height (PBLH) is lower (approximately 400 m, Fig. S2 in the Supplement), and winds are lighter in winter months, compared to summer months, over South Asia, and particularly over IGP region (Surendran et al., 2016). Figure 7 (left) and 7 (right) shows the time-height distribution of NH_3 and mean PBLH averaged over the IGP region, respectively. It can be seen that during winter months higher atmospheric stability prevents mixing of boundary layer $NH_3$to the free troposphere over IGP (Fig. 7 (left)), which is reflected in the higher wintertime values of MOZART-4 NH_3 columns.Similarly, higher NH_3/NH_4 ratio (Fig.S3 in the Supplement) and lower dry and wet deposition (Fig. S4 and S5 in the Supplement) of NH_3 over IGP in winter month enhances the accumulation of NH_3 in the boundary layer compared to summer months. On the other hand, much less NH_3 gets detected by the satellite at the higher altitudes where detection sensitivity of the satellite is more than that at the surface (Clarisse et al., 2010). Limited sensitivity of IASI measurements to detect boundary layer NH_3 (Van Damme et al., 2014a) could be one of the reasons for large differences ($1\text{-}4\times10^{16}$ molecules cm^{-2}) between MOZART-4 and IASI in winter seasons. Also, sowing of wheat crop over IGP involves higher rate of fertilizer application during peak winter month (Sharma et al., 2014) that release significant quantity of NH_3 into the

391 atmosphere. However, this seasonality is largely missing in the emissions (Fig. 2 (top, left)) indicating that
392 higher MOZART-4 NH_3 is largely driven by the winter-time meteorology over this region.
393 It is interesting to note from Fig. 6 (right) that during spring the difference between modelled and observed
394 column NH_3 is smaller over the IGP region compared with the winter season. Heating of the landmass due to
395 large solar incidence suppresses the wintertime subsidence over the IGP and leads to deeper boundary layer
396 during spring and early summer. It can be seen that (Fig. 7 (right) and Fig. S2 in the Supplement) the average
397 PBLH is about 1100 m and 600 m deeper during spring and summer compared to winter over IGP. During this
398 season, significant transport of the boundary pollution in the mid and upper troposphere due to enhanced
399 convective activities and large scale vertical motion can be noticed in Fig. 7 (left) and is consistent with the
400 earlier studies over this region (Lal et al., 2014; Surendran et al., 2016). Vertical motion associated with the
401 convective activities is expected to redistribute the NH_3 concentration in the column, which leads to more NH_3
402 at the higher altitudes where detection sensitivity of the satellite is more than that at the surface (Clarisse et al.,
403 2010). As a result, more NH_3 gets detected by the satellite and we see less difference between observations and
404 model over the IGP. This may also partly explain the higher IASI estimates of NH_3 column for summertime
405 prior to the monsoon season. However, this hypothesis needs to be tested with higher sensitivity experiments as
406 a part of future work. During spring season, MOZART-4 reflects widespread NH_3 total column from the entire
407 Indian land mass and IASI observations does capture increase in NH_3 total column at least for seasonal mean
408 cycle (Fig. 8a). This seasonal maximum in NH_3 total column identified both in IASI and MOZART-4 over
409 South Asia can be explained by the two factors: Meteorology factor and biomass burning emissions.
410 Volatilization of NH_3 enhances with increase in temperature (Sutton et al., 2013), hence higher temperature
411 during this drier periods over IGP partly enhances NH_3 emission to the environment which is also evident from
412 the soil NH_3 emissions in Fig. 2 (bottom). However, magnitude of these emissions is expected to be smaller in
413 comparison with anthropogenic emissions. In the Indian region, emissions from the biomass burning (crop-
414 residue burning) peaks in March to May (Jena et al., 2015a) and emission of NH_3 from biomass burning is
415 maximum during this period (Fig. 2 (middle)). However, MOZART-4 estimates smaller NH_3 total columns
416 compared with IASI over Myanmar, Laos and Thailand during the period March-May (Fig. 6 (right)). This
417 period is estimated to be associated with large scale forest fires (and open crop burning) (Chan, 2017; Wu et al.,
418 2018; Zheng et al., 2017), the effect of which appears to be underestimated in the MOZART-4 simulations. It
419 suggests that the Global Fire Emissions Database (GFED-v3) used in this study is low over this region agreeing
420 with Zhang et al. (2020) and Huang et al. (2013). During the monsoon season (JJA) (Fig. 6 (right)) and summer,
421 IASI-NH_3 total columns are larger than the MOZART-4 estimates over north-western arid region of South Asia,
422 where monsoon rainfall is lowest (less than 30 cm). On the other hand, NH_3 columns estimated by IASI are
423 lower in the North-western IGP than the MOZART-4 simulations.
424 Figure 8 shows the comparison between IASI and modelled monthly time series of NH_3 total columns over IGP
425 (20°N-32°N, 70°E-95°E) and NCP (30°N-40°N, 110°E-120°E), respectively (rectangular areas shown on Fig.
426 1). We found a better consistency between modelled and measured seasonal NH_3 total column over NCP than
427 IGP. Monthly NH_3 columns over the IGP show bimodal distribution in the model. However, IASI does not
428 show such bimodal variation. Seasonal statistics show large normalised mean bias (38 %) and poor correlation (r
429 = 0.41) between model and IASI. The bimodal distribution in NH_3 total columns is partly driven by the biomass
430 burring emissions, which show major peak in spring and another small peak in autumn (Fig. 2 (middle)), and

partly by the meteorology as discussed in the previous section. During monsoon months (JJA), when South Asia receives significant rainfall all over, model simulations present lower NH_3 total column, which is not seen in the IASI observations and also in the surface observations (Fig. 8a and 9b) over IGP. The reason for this discrepancy may be related with the flat NH_3 emission over South Asia (Fig. 2). Usually large amount of fertilization application is expected during the warm month of June and July in the IGP which is not represented in the HTAP-v2 emissions and therefore lower values in the model during monsoon month is mostly driven by the model meteorology. Lower values observed during monsoon season in general are attributed to increase wet scavenging of NH_3 due to monsoon rain (Fig. S5 (left) in the Supplement) and influx of cleaner marine air from the Bay of Bengal and Arabian Sea through south-easterly and south-westerly wind (Ghude et al., 2008). On the other hand, monthly variation in IASI NH_3 total columns over East Asia is found to be captured well by the model (Fig. 8b) and seems to follow the variation observed in the anthropogenic NH_3 emission (Fig. 2), except for the month of July where IASI estimates substantially higher NH_3 total columns than the model. The reason for this peak in the IASI data for July may be related to urea fertilizer application in warm July conditions (see temporal course of Enhanced Vegetation Index (Li et al., 2014)), which seems to be not represented well in the HTAP-v2 emissions. The overall statistics show slight good correlation (r = 0.61) between observed and simulated NH_3 columns and negative normalised mean bias (NMB = -41 %).

3.3 Comparison between surface NH_3 measurements and simulated NH_3 concentrations in South and East Asia

To evaluate modelled surface NH_3 concentrations in South Asia, we have used NH_3 surface measurements from 69 monitoring locations over India for the years from 2016 to 2019. As 2010 data was not available, we make the hypothesis that measurement from 2016-2019 can be considered as representative from what have been measured in 2010. Out of these stations thirty five locations in Delhi, six in Bangalore city, four in Hyderabad, and two in Jaipur city are averaged to get singe value for the same geographical location and the remaining 22 locations are considered independently representing 26 respective cities. Due to the lack of ground-based measurements performed in 2010, the following comparison will mainly be qualitative, although it is estimated that the main spatial features of Indian agriculture and NH_3 emissions will be consistent between 2010 and 2016-2019. As per the RCP 8.5 (Kumar et al., 2018) NH_3 emission from South Asia is expected to increase by less than 20 % from 2010 to 2020. Assuming a linear relationship between emission and surface concentration, it is expected that NH_3 concentrations could be higher by about 10-15 % in 2016 to 2019.

It is interesting to note that the correlation between annual and monthly mean MOZART-4 simulated and measured NH_3 concentration (r = 0.82 and r = 0.62) is better than the comparison between MOZART-4 and IASI for South Asia (Fig. 9). However, the MOZART-4 has systematically smaller estimated NH_3 concentrations compared with the ground based measurement network (NMB = -47 %). It should be noted that most of the monitoring stations are situated in urban regions(cities) of India and therefore represents the urban environment, which may have locally higher NH_3 concentrations due to traffic and human activities (Sharma et al., 2014). Since the MOZART-4 model is run relatively at coarse (1.9° × 2.5°) grid resolution the emissions may not capture the true variability in emissions at city scale. These surface NH_3 sites are influenced by local emissions that are therefore not resolved by the MOZART-4 model. Therefore, when comparing coarse-scale models to observations, the model may have difficulties in resolving local scales effects (Surendran et al., 2015). Until the planned further evaluation of the chemiluminescence monitoring method for ammonia (measured by

difference with NOx) is evaluated (as noted in Sect. 2.4), it is not possible to be certain the extent to which possible uncertainties in the measurement method contribute to the differences shown in Fig. 9b. While noting these uncertainties, it is worth noting that the ground based NH_3 observation network confirms the occurrence of higher ground-level NH_3 concentrations in autumn and winter, as simulated using MOZART-4 using the HTAP-v2 emissions inventory (Fig. 9b).

Comparison of Fig. 8a and 9b shows that the time course of ground level NH_3 concentrations (as estimated by MOZART-4) is significantly different to the time course of total NH_3 column (as also estimated by MOZART-4). Whereas the total column is largest in the summer (reflective of deeper atmospheric mixing and recirculation), and the ground level concentrations are largest during winter. Although it is not easy to use the IASI data to infer ground level NH_3 concentrations, the stronger summer maximum of IASI (Fig. 8a) compared with MOZART-4, suggests that IASI would be in less close agreement with the ground based measurement network than MOZART-4 (Fig. 9b). While recognizing uncertainties in this interpretation, the key point is that large NH_3 columns estimated by IASI for May-July are not reflected in the ground-based NH_3 measurements from the Indian monitoring network.

Figure 10 shows the comparison between monthly mean (from 2010 to 2015 observations) NH_3 surface measurements from 32 monitoring locations over China and modelled surface NH_3 concentrations from the same location over East. Similar to South Asia the MOZART-4 has systematically smaller estimated NH_3 concentrations compared with the ground based measurement network (NMB = -44 %) over East Asia. Figure 10b shows maximum NH_3 concentration occurred in summer (JJA) denotes agreement with IASI measurements. Other statistical indicators are summarised in Table 2. Furthermore, high NH_3 concentration from ground based measurements during JJA is consistent with the higher HTAP-v2 emissions (Fig. 2) (Huang et al., 2012) and higher NH_4NO_3 concentration (Fig. S6 in the Supplement). Higher concentration of NH_4NO_3 and can also lead to higher NH_3 concentrations especially during summer due to its semi-volatile and unstable character at higher temperatures, as it is observed in East Asia. This implies that the NH_3 emissions may play a vital role in determining the seasonal pattern of the ground NH_3 concentrations. Summer peak may originate from fertilizer application, livestock emissions and volatilization of NH_3 which is enhanced in higher temperature (Liu et al., 2017a).

3.4 Why were NH_3 total columns low over high NH_3 emission over East Asia compared to high NH_3 emission region of South Asia?

Fine-scale details of the NH_3 emissions over Asia in Fig. 1 and 2 clearly revealed larger emission values in areas where there is intensive agricultural management. This is the case especially in the NCP and IGP (Fig. 1, shown with box). Earlier emission estimates suggest that fertilizer application and livestock contribute 2.6 Tg per year (yr^{-1}) and 1.7 Tg yr^{-1} NH_3 emissions respectively from South Asia (Aneja et al., 2011). Over South Asia, urea accounts for emissions of 2.5 Tg yr^{-1} which contributes to 95 % of the fertilizer emission, and 58 % of total estimated agricultural emissions (Fertlizer Association of India annual report 2018-19). For East Asia, livestock manure management accounts for approximately 54 % (5.3 Tg yr^{-1}) of the total emissions and fertilizer application accounts for 33 % (3.2 Tg yr^{-1}) emissions, with 13 % of emissions from other sources. Combined the model areas for NCP and IGP (as shown in Fig. 1) accounts for ~45 % of the NH_3 emitted from fertilization in East Asia and South Asia (Huang et al., 2012).

We find that satellite observations show larger NH_3 columns over IGP than over similar higher emission regions of NCP. However, in addition, we also find that the MOZART-4 model is able to capture this contrasting columnar NH_3 levels between IGP and NCP. This indicates that the difference between IGP and NCP is unrelated to differences between the mosaic of emissions over South Asia and East Asia in HTAP-v2 and similarly not related to uncertainties in satellite retrievals. Instead, the analysis from MOZART-4 demonstrates that the difference can be explained by differences in atmospheric chemistry between the two regions, linked to higher SO_2 and NO_x emissions in the NCP than in the IGP. Recent study by Wang et al. (2020), shows that emission fluxes of SO_2 and NO_x over IGP are only one-fourth of that over NCP.

As ammonia is a highly alkaline gas with an atmospheric lifetime usually of few hours (and rarely a few days) (Dammers et al., 2019), it readily reacts with acid present in the atmosphere to form aerosols, which are eventually deposited to the earth's surface by either dry or wet deposition processes (Fig. S4 and S5 in the Supplement). In the atmosphere, ammonia therefore reacts rapidly with atmospheric sulphuric acid (H_2SO_4), nitric acids (HNO_3) and hydrochloric acid (HCl) to contribute to ambient levels of fine particles, forming ammonium sulphate, ammonium nitrate and ammonium chloride. Following reaction (R1) and (R2)

$$NH_{3(g)} + HNO_{3(g)} \leftrightarrow NH_4NO_{3(s)} \quad \text{(R1)}$$

$$2NH_{3(g)} + H_2SO_{4(g)} \leftrightarrow (NH_4)_2SO_{4(s)} \quad \text{(R2)}$$

In the atmosphere, ammonium ion (NH_4^+) as an aerosol is estimated to have a lifetime of about 1–15 days (Aneja et al., 1998), though this is obviously dependent on the amount of atmospheric acids (Seinfeld and Pandis, 2012). In addition to the large fertilizer application and livestock management activities which are characteristic of both IGP and NCP, industrial and transportation activities are higher over the NCP (China) which also results in higher emission of NO_x and SO_2 over NCP compared with IGP (Zhao et al., 2013). Ammonia has greater affinity towards oxides of sulphur, hence it first reacts to form ammonium sulphate, and then the remaining ammonia further reacts to form ammonium nitrate (Seinfeld et al., 1998). The differences in the secondary aerosol formation over NCP and IGP are compared by considering the MOZART-4 model estimates of volume mixing ratio (VMR) in parts per billion ($\times 10^9$ ppb) of total sulphate, ammonium, ammonium nitrate at surface and total column of NO_x (Fig. 11). Although vertical profiles of the aerosol components are small, there are strong vertical gradients in NO_x concentrations, and for this reason we consider the comparison with the total NO_x column more reflective of overall NO_x chemistry than the ground level NO_x VMR.

Figure 11 shows that total sulphate VMR (Fig. 11a) and NO_x total column (Fig. 11c) are significantly higher over NCP region than IGP. Similarly, total ammonium VMR (Fig. 11b) is significantly larger over NCP than IGP indicating how a higher fraction of the gaseous ammonia is transformed to form ammonium over NCP region. In addition, Fig. 11d shows higher estimated levels of ammonium nitrate in MOZART-4 over NCP, reflective of the higher NOx emissions in this region. As a consequence of the different SO_2 and NO_x sources, gaseous NH_3 is more quickly removed from atmosphere over East Asia with residence time of approximately 6 hours (Fig. S7 in the Supplement) (higher values indicates lower mean residence time), which is reflected in the higher VMR of ammonium, sulphate and ammonium nitrate (Fig. 11a, b and d). It can be seen that NH_3/NH_4^+ ratio denotes lower values 0-1 (Fig. S3 in the Supplement) over East Asia than South Asia suggesting NH_4^+

549 partitioning is more over East Asia. As a result the NH_3 total columns over NCP are much smaller than over
550 IGP, even though magnitude of NH_3 emission fluxes is greater over NCP than IGP. This difference indicates
551 that the high NH_3 loading over the IGP is partly coming from the low gas-to-particle partitioning of NH_3 caused
552 by low SO_2 and NO_x emission over South Asia. In contrasts high SO_2 and NO_x emissions promote the
553 conversion of gaseous NH_3 into particulate ammonium in NCP. However, rapid decline of acidic (SO_2)
554 emissions over China after 2000, which may not be reflected correctly in HTAP_v2 (Mortier et al., 2020; Tong
555 et al., 2020; Zheng et al., 2018) will lead to higher NH_3 loading due to less partitioning of NH_3.

556 **4. Conclusion**

557 In this work, we have compared NH_3 total columns simulated by the MOZART-4 model with IASI NH_3 satellite
558 observations over South and East Asia. The annual mean distribution reveals a consistent spatial pattern
559 between MOZART-4 and IASI, but MOZART-4 tends to show larger NH_3 columns over South Asia than IASI,
560 particularly over the Indo-Gangetic Plain (IGP), whereas it is in close agreement over East Asia (including the
561 North China Plain, NCP), with the exception of a July peak seen in the IASI dataset, which may be related to
562 specific timing of fertilizer-related NH_3 emissions. Comparison for seasonally and monthly resolved IASI total
563 column with the MOZART-4 simulations shows inconsistencies in spatial and temporal pattern over South Asia.
564 This inconsistency is due to the uncertainties in emission estimate which doesn't include seasonality pattern in
565 HTAP-v2 over South Asia, as well as uncertainties in the processing of the IASI data. Both the MOZART-4
566 results and IASI estimates involve assumptions that could considerably affect the comparison between total
567 columns of NH_3.
568 Comparison with estimates from a ground based NH_3 monitoring network for both South and East Asia, our
569 results showed that MOZART-4 systematically gives smaller NH_3 concentration estimates than the monitoring
570 network. The NH_3 measurement sites used in present study mostly represent urban locations and model may not
571 be able to capture actual concentration at point location due to coarser grid resolution over India. In addition,
572 further assessment is needed to demonstrate the reliability of the NH_3 measurement technique used in the
573 monitoring network, where NH_3 is measured by difference with NO_x concentrations, which may be uncertain in
574 urban areas with high NO_x concentrations.
575 Despite the high NH_3 emission over both South and East Asia, a larger NH_3 total column is observed over South
576 Asia in both the IASI and MOZART-4 estimates. This difference is explained by the MOZART-4 simulation,
577 which treat the full atmospheric chemistry interaction with SO_2 and NO_x emissions, leading to aerosol
578 formation. The MOZART-4 model showed higher sulphate volume mixing ratio and NO_x total column over East
579 Asia, especially in the NCP, which is reflected in ammonium aerosol volume mixing ratio (VMR) over East
580 Asia. This suggests that the formation of ammonium aerosols (dominated by ammonium, sulphate and
581 ammonium nitrate) is quicker over East Asia than in South Asia, leading to lower NH_3 total columns in East
582 Asia.
583 To examine the present findings future studies should investigate the effect of changing emissions of NO_x and
584 SO_2 on NH_3 columns, for example by using perturbation of these emissions through counterfactual modeling
585 scenarios. The comparison between model simulations using MOZART-4, satellite derived estimates from IASI
586 and ground-based monitoring of NH_3 concentrations has highlighted the known uncertainties in emissions,
587 satellite retrievals and measurements at point locations. In order to reduce the uncertainties in ammonia

emission, it would be a key to create an NH_3 emission inventory specifically over South Asia, which is now currently under development as part of the GCRF South Asian Nitrogen Hub. This includes work to improve the bottom-up NH_3 emission inventory, taking into account primary agricultural statistics on fertilizer use and animal number distributions. There is also potential for top-down (inverse modelling) for NH_3 and NO_x by taking inference from the model, satellite and ground-based evidence. Here it is essential to recognize the need for more ground-based observational sites to measure NH_3 air concentrations in rural areas where agriculture activity is predominant. Such measurements at present are currently very few for South Asia. Coarser global models fail to resolve the local-scale emissions, hence higher resolution regional models with advance chemistry are also needed to resolve the sources and chemical processes on urban and rural scales.

Data availability

The $0.1^{\circ} \times 0.1^{\circ}$ emission grid maps can be downloaded from the EDGAR website on https://edgar.jrc.ec.europa.eu/htap_v2/index.php?SECURE=_123 per year per sector. The model data can be downloaded upon request from the AeroCom database (http://www.htap.org/, last accessed June 22, 2020) (TF HTAP, 2018). The model data is available at Prithvi (IITM) super-computer and can be provided upon request to corresponding author. The morning overpass NH_3 total columns measured through IASI can be accessed from data center at http://cds-espri.ipsl.upmc.fr/etherTypo/index.php?id=1700&L=1. For India, ground based hourly NH_3 measurements can be obtained from CPCB website on https://app.cpcbccr.com/ccr. For China, ground based monthly mean NH_3 datasets can be downloaded from https://figshare.com/articles/Data_Descriptor_Xu_et_al_20181211_Scientific_data_docx/7451357.

Author contributions

All authors contributed to the research; SDG designed the research; PVP conducted the research; PVP and SDG wrote the paper; CJ and DS performed the MOZART model simulations; AM and MAS formulated the research; MVD, LC and PFC performed the IASI experiments; SK, DML, GG, XL, WU, JJ and TKA contributed to writing.

Competing interests

The authors declare that they have no conflict of interest.

Acknowledgments

We wish to thank the National Centre for Atmospheric Research (NCAR), funded by the U.S. National Science Foundation and operated by the University Corporation for Atmospheric Research, for access to the MOZART-4. All model runs were carried out on a Prithvi IBM High Performance Computing system at the Indian Institute of Tropical Meteorology (IITM), Pune India. We thank the Director, IITM for providing all the essential facilities required to complete the work. We wish to acknowledge the availability of CPCB data from CPCB webportal (https://app.cpcbccr.com/ccr).Research at ULB has been supported by the Belgian State Federal

Office for Scientific, Technical and Cultural Affairs (Prodex arrangement IASI.FLOW). L.C. and M.V.D are respectively research associate and postdoctoral researcher with the Belgian F.R.S-FNRS. Cooperation between IITM and CEH has been facilitated through the NEWS India-UK Virtual Joint Centre, supported at CEH by the Biotechnological and Biological Sciences Research Council, and the Natural Environment Research Council of UK Research and Innovation (UKRI), and through the UKRI Global Challenges Research Fund (GCRF) South Asian Nitrogen Hub. The Nationwide Nitrogen Deposition Monitoring Network (NNDMN) of China was supported by the Chinese National Natural Science Foundation (41425007) and the Chinese National Research Program for Key Issues in Air Pollution Control (DQGG0208).We thank anonymous reviewers and the editor for their constructive comments that helped in improving quality of this manuscript.

Financial support

This research has been supported by “Urban modeling C-DAC” sponsored project.

References

Acharja, P., Ali, K., Trivedi, D. K., Safai, P. D., Ghude, S., Prabhakaran, T. and Rajeevan, M.: Characterization of atmospheric trace gases and water soluble inorganic chemical ions of PM_1 and $PM_{2.5}$ at Indira Gandhi International Airport, New Delhi during 2017–18 winter, Sci. Total Environ., 729, 138800, doi:10.1016/j.scitotenv.2020.138800, 2020.

Alexandratos, N. and Bruinsma, J.: World Agriculture Towards 2030 / 2050 The 2012 Revision. Global Perspective Studies Team, FAO Agricultural Development Economics Division. ESA Working Paper No. 12-03, , (12) [online] Available from: http://www.fao.org/docrep/016/ap106e/ap106e.pdf, 2012.

Aneja, V. P., Murray, G. C. and Southerland, J.: Atmospheric nitrogen compounds: Emissions, transport, transformation, deposition, and assessment, EM Air Waste Manag. Assoc. Mag. Environ. Manag., 22–25, 1998.

Aneja, V. P., Battye, W., Behera, S. N., Erisman, J. W., Schlesinger, W. H. and Sharma, M.: Reactive nitrogen emissions from crop and livestock farming in India, Atmos. Environ., 47, 92–103, doi:10.1016/j.atmosenv.2011.11.026, 2011.

Battye, W. and B. R.: Review of Ammonia Emission Modeling Techniques for Natural Landscapes and Fertilized Soils, Work Assign. No. 2-09, 27517(68), 2004.

Behera, S. N., Sharma, M., Aneja, V. P. and Balasubramanian, R.: Ammonia in the atmosphere: a review on emission sources, atmospheric chemistry and deposition on terrestrial bodies, Environ. Sci. Pollut. Res., 20(11), 8092–8131, doi:10.1007/s11356-013-2051-9, 2013.

Chan, K. L.: Biomass burning sources and their contributions to the local air quality in Hong Kong, Sci. Total Environ., 596–597, 212–221, doi:10.1016/j.scitotenv.2017.04.091, 2017.

Clarisse, L., Clerbaux, C., Dentener, F., Hurtmans, D. and Coheur, P. F.: Global ammonia distribution derived from infrared satellite observations, Nat. Geosci., 2(7), 479–483, doi:10.1038/ngeo551, 2009.

Clarisse, L., Shephard, M. W., Dentener, F., Hurtmans, D., Cady-Pereira, K., Karagulian, F., Van Damme, M., Clerbaux, C. and Coheur, P. F.: Satellite monitoring of ammonia: A case study of the San Joaquin Valley, J. Geophys. Res. Atmos., 115(13), 1–15, doi:10.1029/2009JD013291, 2010.

Clarisse, L., Van Damme, M., Clerbaux, C. and Coheur, P. F.: Tracking down global NH_3 point sources with wind-adjusted superresolution, Atmos. Meas. Tech., 12(10), 5457–5473, doi:10.5194/amt-12-5457-2019, 2019.

659 Clerbaux, C., Boynard, A., Clarisse, L., George, M., Hadji-Lazaro, J., Herbin, H., Hurtmans, D., Pommier, M.,
660 Razavi, A., Turquety, S., Wespes, C. and Coheur, P. F.: Monitoring of atmospheric composition using the
661 thermal infrared IASI/MetOp sounder, Atmos. Chem. Phys., 9(16), 6041–6054, doi:10.5194/acp-9-6041-2009,
662 2009.

663 CPCB: Guidelines for Real Time Sampling & Analyses. [online] Available from:
664 http://www.indiaenvironmentportal.org.in/files/NAAQSManualVolumeII.pdf, 2011.

665 CPCB: Annual Report 2014-15., 2014.

666 CPCB: Central Pollution Control Board (2020), [online] Available from: https://cpcb.nic.in/quality-assurance-
667 quality-control/ (Accessed 26 May 2020), 2020.

668 Crippa, M., Guizzardi, D., Muntean, M., Schaaf, E., Dentener, F., Van Aardenne, J. A., Monni, S., Doering, U.,
669 Olivier, J. G. J., Pagliari, V. and Janssens-Maenhout, G.: Gridded emissions of air pollutants for the period
670 1970-2012 within EDGAR v4.3.2, Earth Syst. Sci. Data, 10(4), 1987–2013, doi:10.5194/essd-10-1987-2018,
671 2018.

672 Van Damme, M., Whitburn, S., Clarisse, L., Clerbaux, C., Hurtmans, D. and Coheur, P.-F.: Version 2 of the
673 IASI NH_3 neural network retrieval algorithm; near-real time and reanalysed datasets, Atmos. Meas. Tech.
674 Discuss., 1–14, doi:10.5194/amt-2017-239, 2017.

675 Van Damme, M., Clarisse, L., Whitburn, S., Hadji-Lazaro, J., Hurtmans, D., Clerbaux, C. and Coheur, P. F.:
676 Industrial and agricultural ammonia point sources exposed, Nature, 564(7734), 99–103, doi:10.1038/s41586-
677 018-0747-1, 2018.

678 Van Damme, Wichink Kruit, R. J., Schaap, M., Clarisse, L., Clerbaux, C., Coheur, P. F., Dammers, E., Dolman,
679 A. J. and Erisman, J. W.: Evaluating 4 years of atmospheric ammonia (NH_3) over Europe using IASI satellite
680 observations and LOTOS-EUROS model results, J. Geophys. Res., 119(15), 9549–9566,
681 doi:10.1002/2014JD021911, 2014a.

682 Van Damme, M.Hurtmans, D., Coheur, P. F., Clerbaux, C., Dolman, A. J., Erisman, J. W., Clarisse, L., Ngadi,
683 Y. and Heald, C. L.: Global distributions, time series and error characterization of atmospheric ammonia (NH_3)
684 from IASI satellite observations, Atmos. Chem. Phys., 14(6), 2905–2922, doi:10.5194/acp-14-2905-2014,
685 2014b.

686 Van Damme, Dammers, E., Flechard, C. R., Coheur, P. F., Xu, W., Erisman, J. W., Galy-Lacaux, C., Neuman,
687 J. A., Clerbaux, C., Van Damme, M.Tang, Y. S., Liu, X., Sutton, M. A., Nowak, J. B. and Clarisse, L.: Towards
688 validation of ammonia (NH_3) measurements from the IASI satellite, Atmos. Meas. Tech., 8(3), 1575–1591,
689 doi:10.5194/amt-8-1575-2015, 2015a.

690 Van Damme, Erisman, J. W., Clarisse, L., Dammers, E., Whitburn, S., Clerbaux, C., Dolman, A. J. and Coheur,
691 P.: Worldwide spatiotemporal atmospheric ammonia (NH_3), Geophys. Res. Lett., 1–9,
692 doi:10.1002/2015GL065496.We, 2015b.

693 Dammers, E., McLinden, C. A., Griffin, D., Shephard, M. W., Van Der Graaf, S., Lutsch, E., Schaap, M.,
694 Gainairu-Matz, Y., Fioletov, V., Van Damme, M., Whitburn, S., Clarisse, L., Cady-Pereira, K., Clerbaux, C.,
695 Francois Coheur, P. and Erisman, J. W.: NH_3 emissions from large point sources derived from CrIS and IASI
696 satellite observations, Atmos. Chem. Phys., 19(19), 12261–12293, doi:10.5194/acp-19-12261-2019, 2019.

697 Dao, X., Wang, Z., Lv, Y., Teng, E., Zhang, L. and Wang, C.: Chemical characteristics of water-soluble ions in
698 particulate matter in three metropolitan areas in the North China Plain, PLoS One, 9(12), 1–16,
699 doi:10.1371/journal.pone.0113831, 2014.

700 Datta, A., Sharma, S. K., Harit, R. C., Kumar, V., Mandal, T. K. and Pathak, H.: Ammonia emission from
701 subtropical crop land area in india, Asia-Pacific J. Atmos. Sci., 48(3), 275–281, doi:10.1007/s13143-012-0027-
702 1, 2012.

703 Dlugokencky, E. J., Myers, R. C., Lang, P. M., Masarie, K. A., Crotwell, A. M., Thoning, K. W., Hall, B. D.,
704 Elkins, J. W. and Steele, L. P.: Conversion of NOAA atmospheric dry air CH_4 mole fractions to a

gravimetrically prepared standard scale, J. Geophys. Res. D Atmos., 110(18), 1–8, doi:10.1029/2005JD006035, 2005.

Emmons, L. K., Walters, S., Hess, P. G., Lamarque, J. F., Pfister, G. G., Fillmore, D., Granier, C., Guenther, A., Kinnison, D., Laepple, T., Orlando, J., Tie, X., Tyndall, G., Wiedinmyer, C., Baughcum, S. L. and Kloster, S.: Description and evaluation of the Model for Ozone and Related chemical Tracers, version 4 (MOZART-4), Geosci. Model Dev., 3(1), 43–67, doi:10.5194/gmd-3-43-2010, 2010.

Fertlizer Association of India annual report 2018-19: Fertlizer Association of India annual report 2018-19., 2018.

Ghude, S. D., Fadnavis, S., Beig, G., Polade, S. D. and van der A, R. J.: Detection of surface emission hot spots, trends, and seasonal cycle from satellite-retrieved NO_2 over India, J. Geophys. Res., 113(D20), D20305, doi:10.1029/2007JD009615, 2008.

Ghude, S. D., Lal, D. M., Beig, G., van der A, R. and Sable, D.: Rain-Induced Soil NO_x Emission From India During the Onset of the Summer Monsoon: A Satellite Perspective, J. Geophys. Res., 115(D16), D16304, doi:10.1029/2009JD013367, 2010.

Ghude, S. D., Beig, G., Kulkarni, P. S., Kanawade, V. P., Fadnavis, S., Remedios, J. J. and Kulkarni, S. H.: Regional co pollution over the Indian-subcontinent and various transport pathways as observed by mopitt, Int. J. Remote Sens., 32(21), 6133–6148, doi:10.1080/01431161.2010.507796, 2011.

Ghude, S. D., Kulkarni, S. H., Jena, C., Pfister, G. G., Beig, G., Fadnavis, S. and Van Der, R. J.: Application of satellite observations for identifying regions of dominant sources of nitrogen oxides over the indian subcontinent, J. Geophys. Res. Atmos., 118(2), 1075–1089, doi:10.1029/2012JD017811, 2013.

Ghude, S. D., Chate, D. M., Jena, C., Beig, G., Kumar, R., Barth, M. C., Pfister, G. G., Fadnavis, S. and Pithani, P.: Premature mortality in India due to $PM_{2.5}$ and ozone exposure, Geophys. Res. Lett., 43(9), 4650–4658, doi:10.1002/2016GL068949, 2016.

Ghude, S. D., Bhat, G. S., Prabhakaran, T., Jenamani, R. K., Chate, D. M., Safai, P. D., Karipot, A. K., Konwar, M., Pithani, P., Sinha, V., Rao, P. S. P., Dixit, S. A., Tiwari, S., Todekar, K., Varpe, S., Srivastava, A. K., Bisht, D. S., Murugavel, P., Ali, K., Mina, U., Dharua, M., Rao, Y. J., Padmakumari, B., Hazra, A., Nigam, N., Shende, U., Lal, D. M., Chandra, B. P., Mishra, A. K., Kumar, A., Hakkim, H., Pawar, H., Acharja, P., Kulkarni, R., Subharthi, C., Balaji, B., Varghese, M., Bera, S. and Rajeevan, M.: Winter fog experiment over the Indo-Gangetic plains of India, Curr. Sci., 112(4), doi:10.18520/cs/v112/i04/767-784, 2017.

Guenther, A., Karl, T., Harley, P., Wiedinmyer, C., Palmer, P. I. and Geron, C.: Estimates of global terrestrial isoprene emissions using MEGAN (Model of Emissions of Gases and Aerosols from Nature), Atmos. Chem. Phys., 6(11), 3181–3210, doi:10.5194/acp-6-3181-2006, 2006.

Han, X., Zhu, L., Liu, M., Song, Y. and Zhang, M.: Numerical analysis of the impact of agricultural emissions on PM2.5 in China using a high-resolution ammonia emissions inventory, Atmos. Chem. Phys., (March), 1–31, doi:10.5194/acp-2019-1128, 2020.

Huang, K., Fu, J. S., Hsu, N. C., Gao, Y., Dong, X., Tsay, S. C. and Lam, Y. F.: Impact assessment of biomass burning on air quality in Southeast and East Asia during BASE-ASIA, Atmos. Environ., 78(2012), 291–302, doi:10.1016/j.atmosenv.2012.03.048, 2013.

Huang, X., Song, Y., Li, M., Li, J., Huo, Q., Cai, X., Zhu, T., Hu, M. and Zhang, H.: A high-resolution ammonia emission inventory in China, Global Biogeochem. Cycles, 26(1), 1–14, doi:10.1029/2011GB004161, 2012.

Janssens-Maenhout G., Dentener F., Van Aardenne J., Monni S., Pagliari V., Orlandini L., Klimont Z., Kurokawa J., Akimoto H., Ohara T., Wankmueller R., Battye B., Grano D., Zuber A., K. T. .: EDGAR-HTAP: a Harmonized Gridded Air Pollution Emission Dataset Based on National Inventories, Ispra (Italy): European Commission Publications Office, , (February), 1–18, doi:ISBN 978-92-79-23122-0, ISSN 1831-9424, 2012.

Janssens-Maenhout, G., Dentener, F. J., Aardenne, J. Van, Monni, S., Pagliari, V., Orlandini, L., Klimont, Z.,

751 Kurokawa, J., Akimoto, H., Ohara, T., Wankmüller, R., Battye, B., Grano, D., Zuber, A. and Keating, T.:
752 EDGAR-HTAP: a harmonized gridded air pollution emission dataset based on national inventories., 2012.

753 Janssens-Maenhout, G., Koffi, B., Crippa, M., Pouliot, G., Zhang, Q., Wankmüller, R., Frost, G., Dentener, F.,
754 Li, M., Guizzardi, D., Denier van der Gon, H., Darras, S., Kuenen, J. J. P., Keating, T., Klimont, Z., Kurokawa,
755 J. and Muntean, M.: HTAP_v2.2: a mosaic of regional and global emission grid maps for 2008 and 2010 to
756 study hemispheric transport of air pollution, Atmos. Chem. Phys., 15(19), 11411–11432, doi:10.5194/acp-15-
757 11411-2015, 2015.

758 Jena, C., Ghude, S. D., Pfister, G. G., Chate, D. M., Kumar, R., Beig, G., Surendran, D. E., Fadnavis, S. and Lal,
759 D. M.: Influence of springtime biomass burning in South Asia on regional ozone (O_3): A model based case
760 study, Atmos. Environ., 100, 37–47, doi:10.1016/j.atmosenv.2014.10.027, 2015a.

761 Jena, C., Ghude, S. D., Beig, G., Chate, D. M., Kumar, R., Pfister, G. G., Lal, D. M., Surendran, D. E.,
762 Fadnavis, S. and van der A, R. J.: Inter-comparison of different NOX emission inventories and associated
763 variation in simulated surface ozone in Indian region, Atmos. Environ., 117, 61–73,
764 doi:10.1016/j.atmosenv.2015.06.057, 2015b.

765 Kumar, R., Barth, M. C., Pfister, G. G., Delle Monache, L., Lamarque, J. F., Archer-Nicholls, S., Tilmes, S.,
766 Ghude, S. D., Wiedinmyer, C., Naja, M. and Walters, S.: How Will Air Quality Change in South Asia by 2050?,
767 J. Geophys. Res. Atmos., 123(3), 1840–1864, doi:10.1002/2017JD027357, 2018.

768 Kurokawa, J., Ohara, T., Morikawa, T., Hanayama, S., Janssens-Maenhout, G., Fukui, T., Kawashima, K. and
769 Akimoto, H.: Emissions of air pollutants and greenhouse gases over Asian regions during 2000-2008: Regional
770 Emission inventory in ASia (REAS) version 2, Atmos. Chem. Phys., 13(21), 11019–11058, doi:10.5194/acp-13-
771 11019-2013, 2013.

772 Kuttippurath, J., Singh, A., Dash, S. P., Mallick, N., Clerbaux, C., Van Damme, M., Clarisse, L., Coheur, P. F.,
773 Raj, S., Abbhishek, K. and Varikoden, H.: Record high levels of atmospheric ammonia over India: Spatial and
774 temporal analyses, Sci. Total Environ., 740, 139986, doi:10.1016/j.scitotenv.2020.139986, 2020.

775 Lal, D. M., Ghude, S. D., Singh, J. and Tiwari, S.: Relationship between Size of Cloud Ice and Lightning in the
776 Tropics, , doi:10.1155/2014/471864, 2014.

777 Lawrence, P. J. and Chase, T. N.: Representing a new MODIS consistent land surface in the Community Land
778 Model (CLM 3.0), J. Geophys. Res. Biogeosciences, 112(1), doi:10.1029/2006JG000168, 2007.

779 Li, L., Friedl, M. A., Xin, Q., Gray, J., Pan, Y. and Frolking, S.: Mapping Crop Cycles in China Using MODIS-
780 EVI Time Series, , (September), doi:10.3390/rs6032473, 2014.

781 Li, M., Zhang, Q., Kurokawa, J., Woo, J., He, K. B., Lu, Z. and Ohara, T.: MIX : a mosaic Asian anthropogenic
782 emission inventory for the MICS-Asia and the HTAP projects, , 34813–34869, doi:10.5194/acpd-15-34813-
783 2015, 2015.

784 Li, M., Zhang, Q., Kurokawa, J. I., Woo, J. H., He, K., Lu, Z., Ohara, T., Song, Y., Streets, D. G., Carmichael,
785 G. R., Cheng, Y., Hong, C., Huo, H., Jiang, X., Kang, S., Liu, F., Su, H. and Zheng, B.: MIX: A mosaic Asian
786 anthropogenic emission inventory under the international collaboration framework of the MICS-Asia and
787 HTAP, Atmos. Chem. Phys., 17(2), 935–963, doi:10.5194/acp-17-935-2017, 2017.

788 Liu, L., Zhang, X., Xu, W., Liu, X., Li, Y., Lu, X., Zhang, Y. and Zhang, W.: Temporal characteristics of
789 atmospheric ammonia and nitrogen dioxide over China based on emission data, satellite observations and
790 atmospheric transport modeling since 1980, Atmos. Chem. Phys., 17(15), 9365–9378, doi:10.5194/acp-17-
791 9365-2017, 2017a.

792 Liu, X., Xu, W., Duan, L., Du, E., Pan, Y., Lu, X., Zhang, L., Wu, Z., Wang, X., Zhang, Y., Shen, J., Song, L.,
793 Feng, Z., Liu, X., Song, W., Tang, A., Zhang, Y., Zhang, X. and Collett, J. L.: Atmospheric Nitrogen Emission,
794 Deposition, and Air Quality Impacts in China: an Overview, Curr. Pollut. Reports, 3(2), 65–77,
795 doi:10.1007/s40726-017-0053-9, 2017b.

796 Mandal, T. K., Saxena, M., Rohtash, Sharma, S. K., Gupta, N. C., Kumar, M. and Saraswati: Characteristics of

ambient ammonia over Delhi, India, Meteorol. Atmos. Phys., 124(1–2), 67–82, doi:10.1007/s00703-013-0299-8, 2013.

Metzger, S., Dentener, F., Pandis, S. and Lelieveld, J.: Gas/aerosol partitioning: 1. A computationally efficient model, J. Geophys. Res. Atmos., 107(16), doi:10.1029/2001JD001102, 2002.

Metzger, S., Mihalopoulos, N. and Lelieveld, J.: Importance of mineral cations and organics in gas-aerosol partitioning of reactive nitrogen compounds: Case study based on MINOS results, Atmos. Chem. Phys., 6(9), 2549–2567, doi:10.5194/acp-6-2549-2006, 2006.

Móring, A., Hooda, S., Raghuram, N., Adhya, T. K., Ahmad, A., Bandyopadhyay, S. K., Barsby, T., Beig, G., Bentley, A. R., Bhatia, A., Dragosits, U., Drewer, J., Foulkes, J., Ghude, S. D., Gupta, R., Jain, N., Kumar, D., Kumar, R. M., Ladha, J. K., Mandal, P. K., Neeraja, C. N., Pandey, R., Pathak, H., Pawar, P., Pellny, T. K., Poole, P., Price, A., Rao, D. L. N., Reay, D. S., Singh, N. K., Sinha, S. K., Srivastava, R. K., Shewry, P., Smith, J., Steadman, C. E., Subrahmanyam, D., Surekha, K., Venkatesh, K., Varinderpal-Singh, Uwizeye, A., Vieno, M. and Sutton, M. A.: Nitrogen Challenges and Opportunities for Agricultural and Environmental Science in India, Front. Sustain. Food Syst., 5, 13, doi:10.3389/fsufs.2021.505347, 2021.

Mortier, A., Gliß, J., Schulz, M., Aas, W., Andrews, E., Bian, H., Chin, M., Ginoux, P., Hand, J., Holben, B., Zhang, H., Kipling, Z., Kirkevåg, A., Laj, P., Lurton, T., Myhre, G., Neubauer, D., Olivié, D., von Salzen, K., Skeie, R. B., Takemura, T. and Tilmes, S.: Evaluation of climate model aerosol trends with ground-based observations over the last 2~decades -- an AeroCom and CMIP6 analysis, Atmos. Chem. Phys., 20(21), 13355–13378, doi:10.5194/acp-20-13355-2020, 2020.

Oleson, K. W., Lawrence, D. M., Bonan, G. B., Flanner, M. G., Kluzek, E., Lawrence, P. J., … Zeng, X. (2010).: Technical Description of version 4.0 of the Community Land Model (CLM)., 2010.

Pfister, G. G., Emmons, L. K., Hess, P. G., Lamarque, J. F., Orlando, J. J., Walters, S., Guenther, A., Palmer, P. I. and Lawrence, P. J.: Contribution of isoprene to chemical budgets: A model tracer study with the NCAR CTM MOZART-4, J. Geophys. Res. Atmos., 113(5), doi:10.1029/2007JD008948, 2008.

Pinder, R. W., Adams, P. J. and Pandis, S. N.: Ammonia Emission Controls as a Cost-Effective Strategy for Reducing Atmospheric Particulate Matter in the Eastern United States, Environ. Sci. Technol., 41(2), 380–386, doi:10.1021/es060379a, 2007.

Pinder, R. W., Gilliland, A. B. and Dennis, R. L.: Environmental impact of atmospheric NH3 emissions under present and future conditions in the eastern United States, Geophys. Res. Lett., 35(12), doi:10.1029/2008GL033732, 2008.

Pollution, C. and Board, C.: Guidelines for Manual Sampling & Analyses., 2011.

Randerson, J., Werf, G. Van Der, Giglio, L., DAAC, G. C.-O. and 2015, undefined: Global Fire Emissions Database, Version 4.1 (GFEDv4), daac.ornl.gov [online] Available from: https://daac.ornl.gov/cgi-bin/download.pl?ds_id=1293&source=schema_org_metadata (Accessed 26 May 2020), n.d.

Saraswati, George, M. P., Sharma, S. K., Mandal, T. K. and Kotnala, R. K.: Simultaneous Measurements of Ambient NH 3 and Its Relationship with Other Trace Gases, PM 2.5 and Meteorological Parameters over Delhi, India, Mapan - J. Metrol. Soc. India, 34(1), 55–69, doi:10.1007/s12647-018-0286-0, 2019.

Seinfeld, J. H. and Pandis, S. N.: Atmospheric Chemistry and Physics: From Air Pollution to Climate Change, Wiley. [online] Available from: https://books.google.co.in/books?id=J3s30hwn_K0C, 2012.

Seinfeld, J. H., Pandis, S. N. and Noone, K.: Atmospheric Chemistry and Physics: From Air Pollution to Climate Change, Phys. Today, 51(10), 88–90, doi:10.1063/1.882420, 1998.

Sharma, S. K., Saxena, M., Saud, T., Korpole, S. and Mandal, T. K.: Measurement of NH3, NO, NO2 and related particulates at urban sites of indo gangetic plain (IGP) of India, J. Sci. Ind. Res. (India)., 71(5), 360–362, 2012.

Sharma, S. K., Harit, R. C., Kumar, V., Mandal, T. K. and Pathak, H.: Ammonia Emission from Rice-Wheat

842 Cropping System in Subtropical Soil of India, Agric. Res., 3(2), 175–180, doi:10.1007/s40003-014-0107-9,
843 2014a.

844 Sharma, S. K., Kumar, M., Rohtash, Gupta, N. C., Saraswati, Saxena, M. and Mandal, T. K.: Characteristics of
845 ambient ammonia over Delhi, India., 2014b.

846 Someya, Y., Imasu, R., Shiomi, K. and Saitoh, N.: Atmospheric ammonia retrieval from the TANSO-
847 FTS/GOSAT thermal infrared sounder, Atmos. Meas. Tech., 13(1), 309–321, doi:10.5194/amt-13-309-2020,
848 2020.

849 Surendran, D., Jena, C., Beig, G., Chate, D. M. and Ghude, S. D.: Quantifying the sectoral contribution of
850 pollution transport from South Asia during summer and winter monsoon seasons in support of HTAP-2
851 experiment, Atmos. Environ., 145, 60–71, doi:10.1016/j.atmosenv.2016.09.011, 2016.

852 Surendran, D. E., Ghude, S. D., Beig, G., Emmons, L. K., Jena, C., Kumar, R., Pfister, G. G. and Chate, D. M.:
853 Air quality simulation over South Asia using Hemispheric Transport of Air Pollution version-2 (HTAP-v2)
854 emission inventory and Model for Ozone and Related chemical Tracers (MOZART-4), Atmos. Environ., 122,
855 357–372, doi:10.1016/j.atmosenv.2015.08.023, 2015.

856 Sutton, M. A., Reis, S., Riddick, S. N., Dragosits, U., Nemitz, E., Theobald, M. R., Tang, Y. S., Braban, C. F.,
857 Vieno, M., Dore, A. J., Mitchell, R. F., Wanless, S., Daunt, F., Fowler, D., Blackall, T. D., Milford, C.,
858 Flechard, C. R., Loubet, B., Massad, R., Cellier, P., Personne, E., Coheur, P. F., Clarisse, L., Van Damme, M.,
859 Ngadi, Y., Clerbaux, C., Skjøth, C. A., Geels, C., Hertel, O., Kruit, R. J. W., Pinder, R. W., Bash, J. O., Walker,
860 J. T., Simpson, D., Horváth, L., Misselbrook, T. H., Bleeker, A., Dentener, F. and de Vries, W.: Towards a
861 climate-dependent paradigm of ammonia emission and deposition, Philos. Trans. R. Soc. B Biol. Sci.,
862 368(1621), 20130166–20130166, doi:10.1098/rstb.2013.0166, 2013.

863 Sutton, M. A., Drewer, J., Moring, A., Adhya, T. K., Ahmed, A., Bhatia, A., Brownlie, W., Dragosits, U.,
864 Ghude, S. D., Hillier, J., Hooda, S., Howard, C. M., Jain, N., Kumar, D., Kumar, R. M., Nayak, D. R., Neeraja,
865 C. N., Prasanna, R., Price, A., Ramakrishnan, B., Reay, D. S., Singh, R., Skiba, U., Smith, J. U., Sohi, S.,
866 Subrahmanyan, D., Surekha, K., van Grinsven, H. J. M., Vieno, M., Voleti, S. R., Pathak, H. and Raghuram, N.:
867 2 - The Indian Nitrogen Challenge in a Global Perspective, in The Indian Nitrogen Assessment, edited by Y. P.
868 Abrol, T. K. Adhya, V. P. Aneja, N. Raghuram, H. Pathak, U. Kulshrestha, C. Sharma, and B. Singh, pp. 9–28,
869 Elsevier., 2017a.

870 Sutton, M. A., J. Drewer, A. Moring, T.K Adhya, A. Ahmed and A. Bhatia: The Indian nitrogen assessment :
871 sources of reactive nitrogen, environmental and climate effects, management options, and policies, in The
872 Indian Nitrogen Assessment, edited by Y. P. Abrol, T. K. Adhya, V. P. Aneja, N. Raghuram, H. Pathak, U.
873 Kulshrestha, C. Sharma, and B. Singh, pp. 9–25, Elsevier., 2017b.

874 Technical specifications for CAAQM station: Technical Specifications For Continuous Ambient Air Quality
875 Monitoring (CAAQM) Station (Real Time) Central Pollution Control Board East Arjun Nagar, Shahdara., 2019.

876 Technical Specifications for Continuous Real Time Ambient Air Quality Monitoring Analysers: Technical
877 Specifications for Continuous Real Time Ambient Air Quality Monitoring Analysers / Station Volume – Ii.,
878 2016.

879 The Global Challenges Research Fund (GCRF) South Asia Nitrogen hub: The Global Challenges Research
880 Fund (GCRF) project, [online] Available from: https://gtr.ukri.org/projects?ref=NE/S009019/1, n.d.

881 Tie, X., Brasseur, G., Emmons, L., Horowitz, L. and Kinnison, D.: Effects of aerosols on tropospheric oxidants:
882 A global model study, J. Geophys. Res. Atmos., 106(D19), 22931–22964, doi:10.1029/2001JD900206, 2001.

883 Tie, X., Madronich, S., Walters, S., Zhang, R., Rasch, P. and Collins, W.: Effect of clouds on photolysis and
884 oxidants in the troposphere, , 108, doi:10.1029/2003JD003659, 2003.

885 Tie, X., Madronich, S., Walters, S., Edwards, D. P., Ginoux, P., Mahowald, N., Zhang, R. Y., Lou, C. and
886 Brasseur, G.: Assessment of the global impact of aerosols on tropospheric oxidants, J. Geophys. Res. D Atmos.,
887 110(3), 1–32, doi:10.1029/2004JD005359, 2005.

Tong, D., Cheng, J., Liu, Y., Yu, S., Yan, L., Hong, C., Qin, Y., Zhao, H., Zheng, Y., Geng, G., Li, M., Liu, F., Zhang, Y., Zheng, B., Clarke, L. and Zhang, Q.: Dynamic projection of anthropogenic emissions in China: methodology and 2015--2050 emission pathways under a range of socio-economic, climate policy, and pollution control scenarios, Atmos. Chem. Phys., 20(9), 5729–5757, doi:10.5194/acp-20-5729-2020, 2020.

Viatte, C., Wang, T., Van Damme, M., Dammers, E., Meleux, F., Clarisse, L., Shephard, M. W., Whitburn, S., Coheur, P. F., Cady-Pereira, K. E. and Clerbaux, C.: Atmospheric ammonia variability and link with particulate matter formation: a case study over the Paris area, Atmos. Chem. Phys., 20(1), 577–596, doi:10.5194/acp-20-577-2020, 2020.

Wang, T., Song, Y., Xu, Z., Liu, M., Xu, T., Liao, W., Yin, L., Cai, X., Kang, L., Zhang, H. and Zhu, T.: Why is the Indo-Gangetic Plain the region with the largest NH_3 column in the globe during pre-monsoon and monsoon seasons?, Atmos. Chem. Phys., 20(14), 8727–8736, doi:10.5194/acp-20-8727-2020, 2020.

Wesely, M. L.: Parameterization of surface resistances to gaseous dry deposition in regional-scale numerical models, Atmos. Environ., 23(6), 1293–1304, doi:10.1016/0004-6981(89)90153-4, 1989.

Whitburn, S., Damme, M. Van, Clarisse, L., Bauduin, S., Heald, C. L., Hurtmans, D., Zondlo, M. A., Clerbaux, C. and Coheur, P.: A flexible and robust neural network IASI-NH_3,, 6581–6599, doi:10.1002/2016JD024828.Received, 2016.

Wu, J., Kong, S., Wu, F., Cheng, Y., Zheng, S., Yan, Q., Zheng, H., Yang, G., Zheng, M., Liu, D., Zhao, D. and Qi, S.: Estimating the open biomass burning emissions in central and eastern China from 2003 to 2015 based on satellite observation, Atmos. Chem. Phys., 18(16), 11623–11646, doi:10.5194/acp-18-11623-2018, 2018.

Xu, J. S., He, J., Behera, S. N., Xu, H. H., Ji, D. S., Wang, C. J., Yu, H., Xiao, H., Jiang, Y. J., Qi, B. and Du, R. G.: Temporal and spatial variation in major ion chemistry and source identification of secondary inorganic aerosols in Northern Zhejiang Province, China, Chemosphere, 179(December 2014), 316–330, doi:10.1016/j.chemosphere.2017.03.119, 2017.

Xu, R. T., Pan, S. F., Chen, J., Chen, G. S., Yang, J., Dangal, S. R. S., Shepard, J. P. and Tian, H. Q.: Half-Century Ammonia Emissions From Agricultural Systems in Southern Asia: Magnitude, Spatiotemporal Patterns, and Implications for Human Health, GeoHealth, 2(1), 40–53, doi:10.1002/2017gh000098, 2018.

Xu, W., Zhang, L. and Liu, X.: A database of atmospheric nitrogen concentration and deposition from the nationwide monitoring network in China, , (December 2018), 2–7, 2019.

Zhang, X., Liu, J., Han, H., Zhang, Y., Jiang, Z., Wang, H., Meng, L., Li, Y. C. and Liu, Y.: Satellite-Observed Variations and Trends in Carbon Monoxide over Asia and Their Sensitivities to Biomass Burning, Remote Sens., 12(5), 830, doi:10.3390/rs12050830, 2020.

Zhang, Y., Dore, A. J., Ma, L., Liu, X. J., Ma, W. Q., Cape, J. N. and Zhang, F. S.: Agricultural ammonia emissions inventory and spatial distribution in the North China Plain, Environ. Pollut., 158(2), 490–501, doi:10.1016/j.envpol.2009.08.033, 2010.

Zhao, B., Wang, S. X., Liu, H., Xu, J. Y., Fu, K., Klimont, Z., Hao, J. M., He, K. B., Cofala, J. and Amann, M.: NOx emissions in China: Historical trends and future perspectives, Atmos. Chem. Phys., 13(19), 9869–9897, doi:10.5194/acp-13-9869-2013, 2013.

Zheng, B., Tong, D., Li, M., Liu, F., Hong, C., Geng, G., Li, H., Li, X., Peng, L., Qi, J., Yan, L., Zhang, Y., Zhao, H., Zheng, Y., He, K. and Zhang, Q.: Trends in China's anthropogenic emissions since 2010 as the consequence of clean air actions, Atmos. Chem. Phys., 18(19), 14095–14111, doi:10.5194/acp-18-14095-2018, 2018.

Zheng, J., Hu, M., Du, Z., Shang, D., Gong, Z., Qin, Y., Fang, J., Gu, F., Li, M., Peng, J., Li, J., Zhang, Y., Huang, X., He, L., Wu, Y. and Guo, S.: Influence of biomass burning from South Asia at a high-altitude mountain receptor site in China, Atmos. Chem. Phys., 17(11), 6853–6864, doi:10.5194/acp-17-6853-2017, 2017.

Zhou, Y., Zhang, Y., Tian, D. and Mu, Y.: Impact of dicyandiamide on emissions of nitrous oxide, nitric oxide

and ammonia from agricultural field in the North China Plain, J. Environ. Sci. (China), 40, 20–27, doi:10.1016/j.jes.2015.08.016, 2016.

Zhu, L., Henze, D. K., Bash, J. O., Cady-Pereira, K. E., Shephard, M. W., Luo, M. and Capps, S. L.: Sources and Impacts of Atmospheric NH3: Current Understanding and Frontiers for Modeling, Measurements, and Remote Sensing in North America, Curr. Pollut. Reports, 1(2), 95–116, doi:10.1007/s40726-015-0010-4, 2015.

FIGURE CAPTIONS

Figure 1. Spatial distribution of total NH_3 emissions ($\times 10^{-10}$ kg $m^{-2}s^{-1}$) over Asia. Data are shown at 0.1° × 0.1° grid resolution from Hemispheric Transport of Air Pollution version-2 (HTAP-v2) emission inventory. The solid rectangles indicate the Indo-Gangetic plain, IGP (20°N-32°N, 70°E-95°E) and the North China Plain, NCP (30°N-40°N, 110°E-120°E).

Figure 2. Monthly variation of anthropogenic (HTAP-v2) (molecules cm^{-2} s^{-1}) (top), Biomass Burning (GEFED-v3) (molecules cm^{-2} s^{-1}) (middle) and Soil (CESM) (molecules cm^{-2} s^{-1}) (bottom) NH_3 emission averaged from Indo-Gangetic plain (20°N-32°N, 70°E-95°E) and the North China Plain (30°N-40°N, 110°E-120°E).

Figure 3. Geographical locations of surface NH_3 observational sites (69 locations) from the air quality automatic monitoring network operated by the Central Pollution Control Board (CPCB, 2020), India and observational sites (32 locations) from Nationwide Nitrogen Deposition Monitoring Network (NNDMN) operated by China Agricultural University, China.

Figure 4. Spatial distributions of annual mean NH_3 ($\times 10^{16}$ molecules cm^{-2}) total columns over Asia for the year 2010. (a) Simulated by MOZART-4, (b) from the IASI satellite observations and (c) spatial difference between MOZART-4 and IASI.

Figure 5. (a) Scatter plot between annual averaged IASI and MOZART-4 simulated NH_3 ($\times 10^{16}$ molecules cm^{-2}) total columns over IGP, South Asia (rectangle: 20°N-32°N, 70°E-95°E) and (b) Scatter plot between annual averaged IASI and MOZART-4 simulated NH_3 ($\times 10^{16}$ molecules cm^{-2}) total columns over NCP, East Asia (rectangle: 30°N-40°N, 110°E-120°E).

Figure 6. Seasonal NH_3 total columns distribution ($\times 10^{16}$ molecules cm^{-2}) in 2010 (left) simulated by MOZART-4, (middle) measured by IASI satellite and (right) spatial differences between MOZART-4 and IASI during (top to bottom) winter (DJF) spring (MAM) summer (JJA) and autumn (SON) seasons.

Figure 7. Daily vertical distribution of NH_3 (ppb) averaged over IGP South Asia (20°N-32°N, 70°E-95°E) (left) and daily mean Planetary Boundary Layer height (PBLH in meters) averaged over IGP South Asia (20°N-32°N, 70°E-95°E) (right).

Figure 8. (a) Comparison between monthly averaged IASI and MOZART-4 simulated NH_3 ($\times 10^{16}$molecules cm^{-2}) total columns over IGP South Asia (20°N-32°N, 70°E-95°E), (b) Comparison of monthly averaged IASI and MOZART-4 simulated NH_3($\times 10^{16}$ molecules cm^{-2}) total columns over NCP East Asia (30°N-40°N, 110°E-120°E) (bar indicates standard error of 88 and 35 pixels in IGP and NCP respectively).

Figure 9. (a) Scatter plot between annual averaged surface observations from 69 monitoring sites (Fig. 2) over South Asia and MOZART-4 simulated surface NH_3 (µg m^{-3}) (992 hPa) interpolated at the locations of 69 sites (b) Comparison between monthly mean surface observations from 69 monitoring sites and MOZART-4 simulated monthly mean NH_3 (µg m^{-3}) concentration interpolated at the locations of 69 sites over South Asia.

Figure 10. (a) Scatter plot between annual averaged surface observations from 32 monitoring sites (Fig. 2) over East Asia and MOZART-4 simulated surface NH_3 (µg m^{-3}) (992 hPa) interpolated at the locations of 32 sites (b) Comparison between monthly mean surface observations from 32 monitoring sites and MOZART-4 simulated monthly mean NH_3 (µg m^{-3}) concentration interpolated at the locations of 32 sites over East Asia.

Figure 11. MOZART-4 simulated spatial distribution of annual averaged (a) total sulphate aerosol ($\times 10^9$ ppb), (b) total Ammonium aerosol ($\times 10^9$ ppb), (c) NO_x total columns ($\times 10^{16}$ molecules cm^{-2}) and (d) total ammonium nitrate aerosol ($\times 10^9$ppb) over Asia.

TABLES

Table 1 Model performance statistics for NH_3 total columns over Asia from IASI and MOZART-4 simulations for the year 2010

Statistics indicator	IGP, South Asia	NCP, East Asia
Mean (Model-IASI) ($\times 10^{16}$ molecules cm^{-2})	0.68	-0.24
Normalized Mean Bias (NMB)	0.38	-0.35
Variance ($\times 10^{16}$ molecules cm^{-2})	1.39	-0.83
Root Mean Square Error (RMSE) ($\times 10^{16}$ molecules cm^{-2})	0.125	0.05
Correlation Coefficient (r)	0.81	0.90

Table 2 Model performance statistics for NH_3 concentration over East and South Asia from MOZART-4 simulations and observational network for the year 2010

Statistics indicator	IGP, South Asia	NCP, East Asia
Mean (Model-Observations) ($\mu g\ m^{-3}$)	-13.47	3.1
Normalized Mean Bias (NMB)	0.44	-0.46
Variance ($\mu g\ m^{-3}$)	-0.629	-0.88
Root Mean Square Error (RMSE) ($\mu g\ m^{-3}$)	1.91	0.728
Correlation Coefficient (r)	0.82	0.65

Figure 1

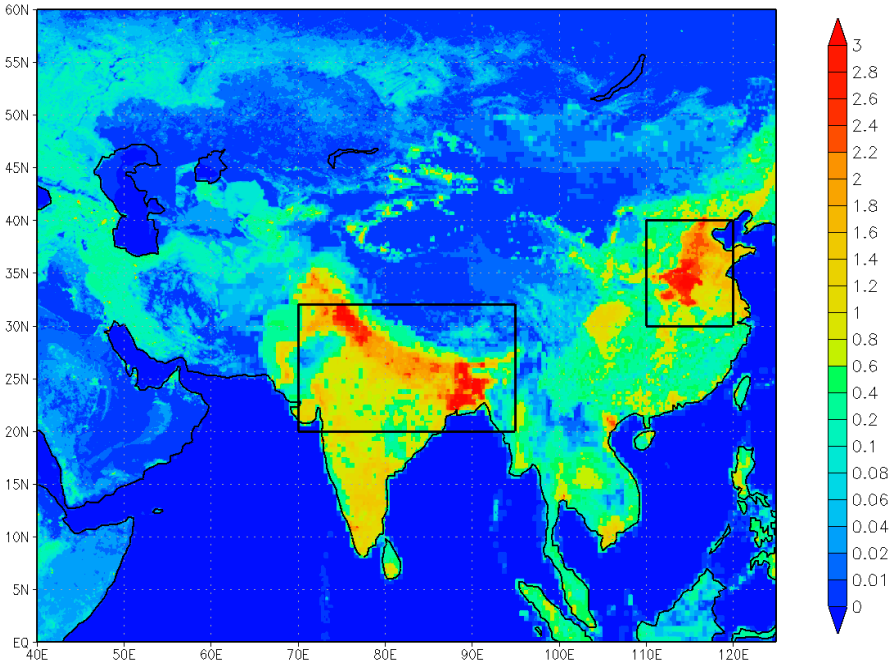
60N
55N
50N
45N
40N
35N
30N
25N
20N
15N
10N
5N
EQ
40E
50E
60E
70E
80E
90E
100E
110E
120E
3
2.8
2.6
2.4
2.2
2
1.8
1.6
1.4
1.2
1
0.8
0.6
0.4
0.2
0.1
0.08
0.06
0.04
0.02
0.01
0

1077 **Figure 2**

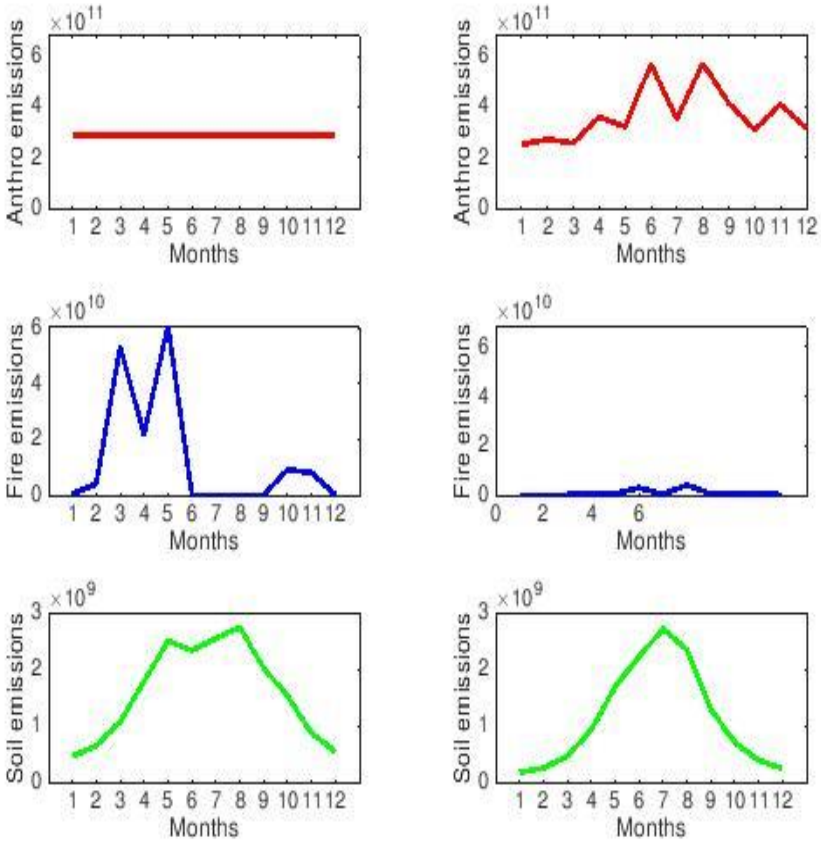

1078

Figure 3

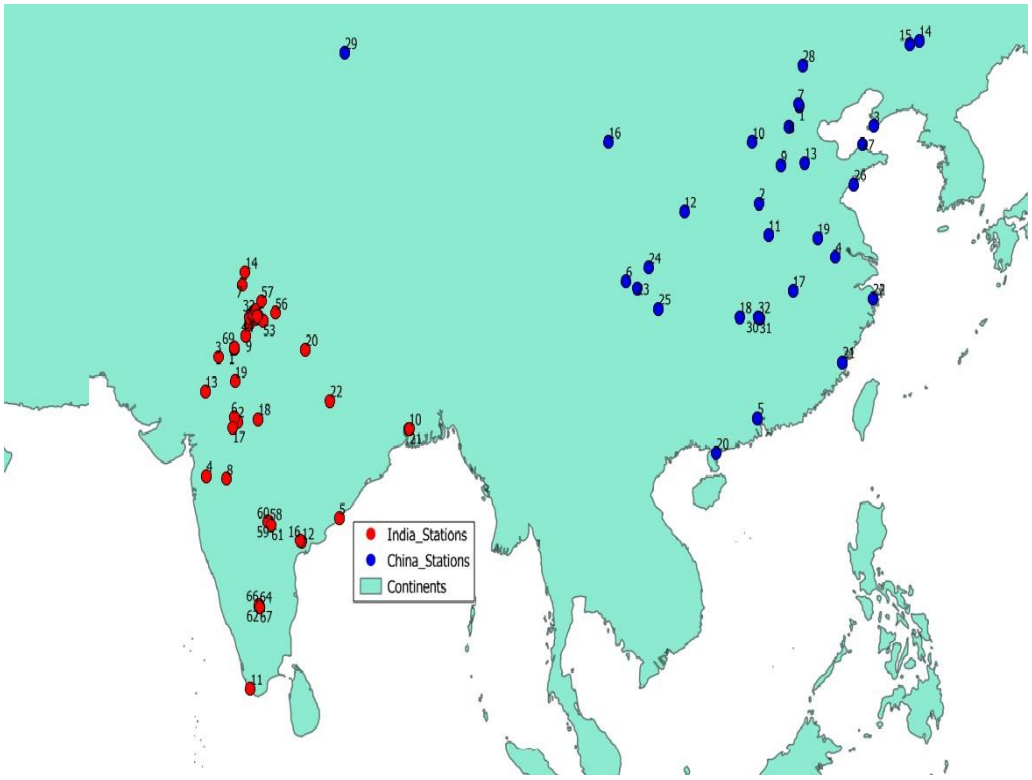

Figure 4

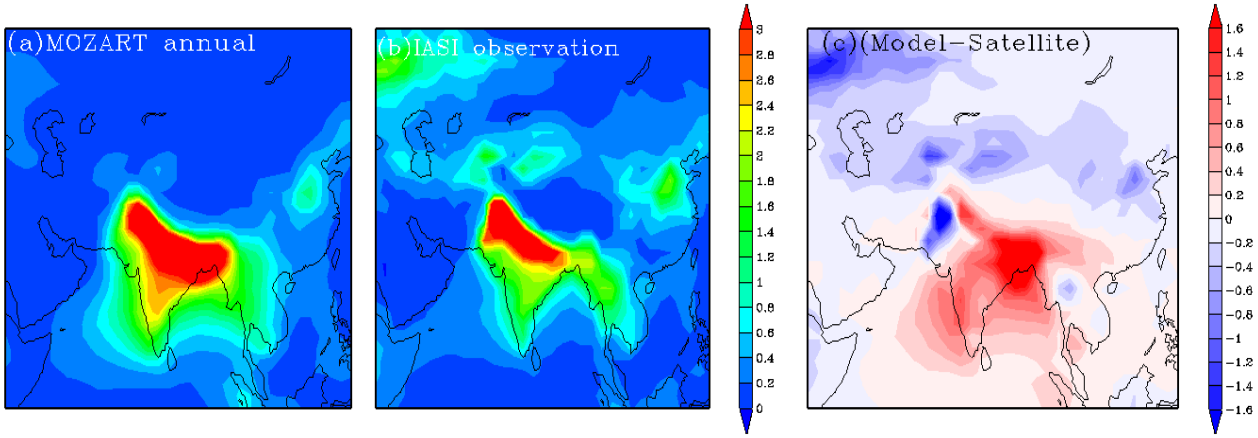
(a)MOZART annual
(b)IASI observation
(c)(Model−Satellite)
3
2.8
2.6
2.4
2.2
2
1.8
1.6
1.4
1.2
1
0.8
0.6
0.4
0.2
0
1.6
1.4
1.2
1
0.8
0.6
0.4
0.2
0
−0.2
−0.4
−0.6
−0.8
−1
−1.2
−1.4
−1.6

Figure 5

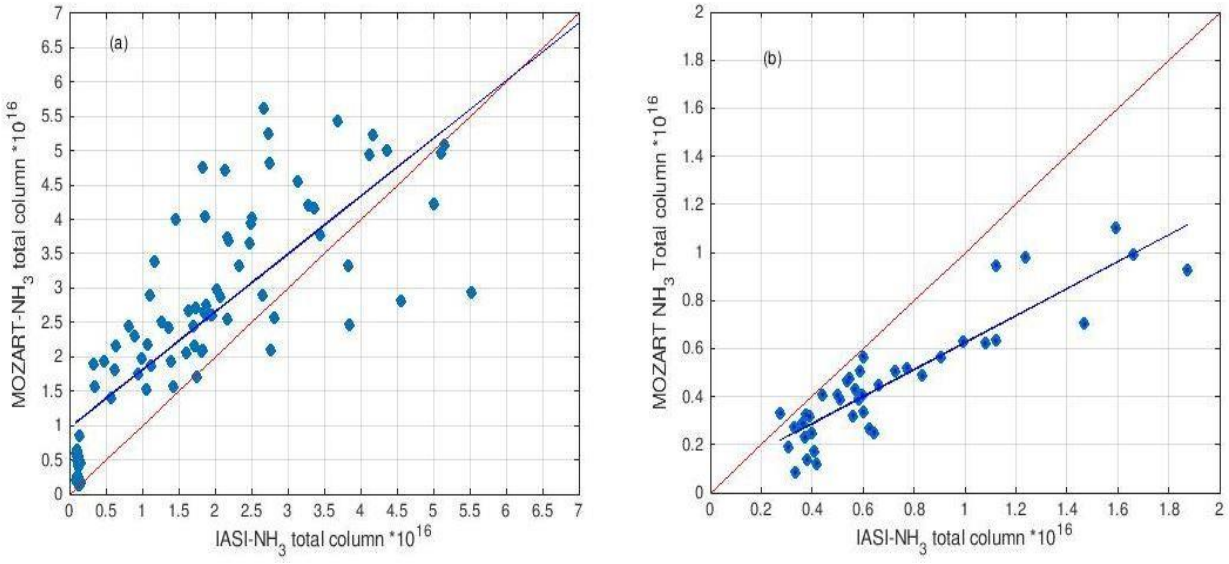
(a)
MOZART-NH3 total column *10^16
IASI-NH3 total column *10^16
(b)
MOZART NH3 Total column *10^16
IASI-NH3 total column *10^16

Figure 6

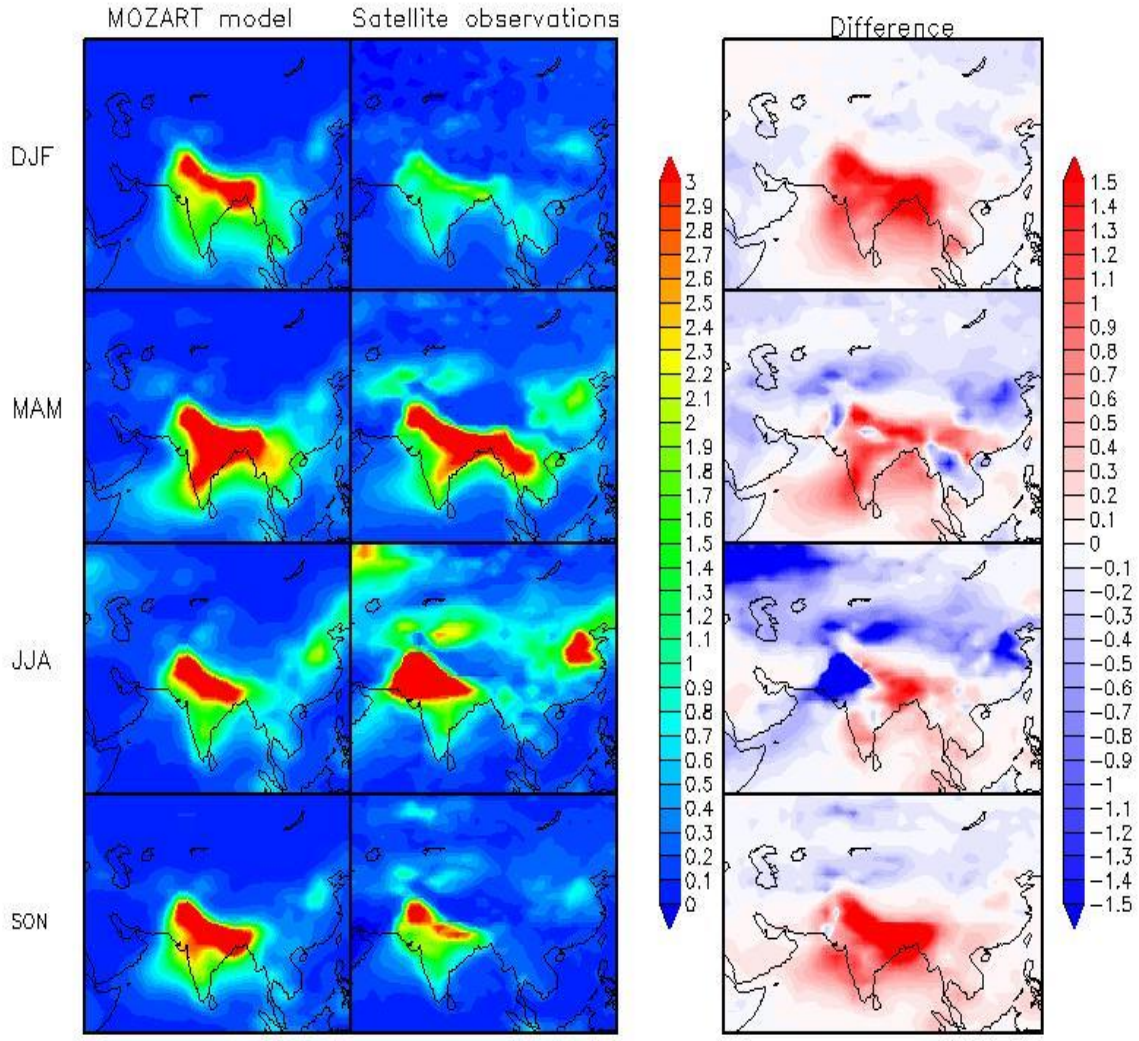
MOZART model
Satellite observations
Difference
DJF
MAM
JJA
SON
3
2.9
2.8
2.7
2.6
2.5
2.4
2.3
2.2
2.1
2
1.9
1.8
1.7
1.6
1.5
1.4
1.3
1.2
1.1
1
0.9
0.8
0.7
0.6
0.5
0.4
0.3
0.2
0.1
0
1.5
1.4
1.3
1.2
1.1
1
0.9
0.8
0.7
0.6
0.5
0.4
0.3
0.2
0.1
0
−0.1
−0.2
−0.3
−0.4
−0.5
−0.6
−0.7
−0.8
−0.9
−1
−1.1
−1.2
−1.3
−1.4
−1.5

Figure 7

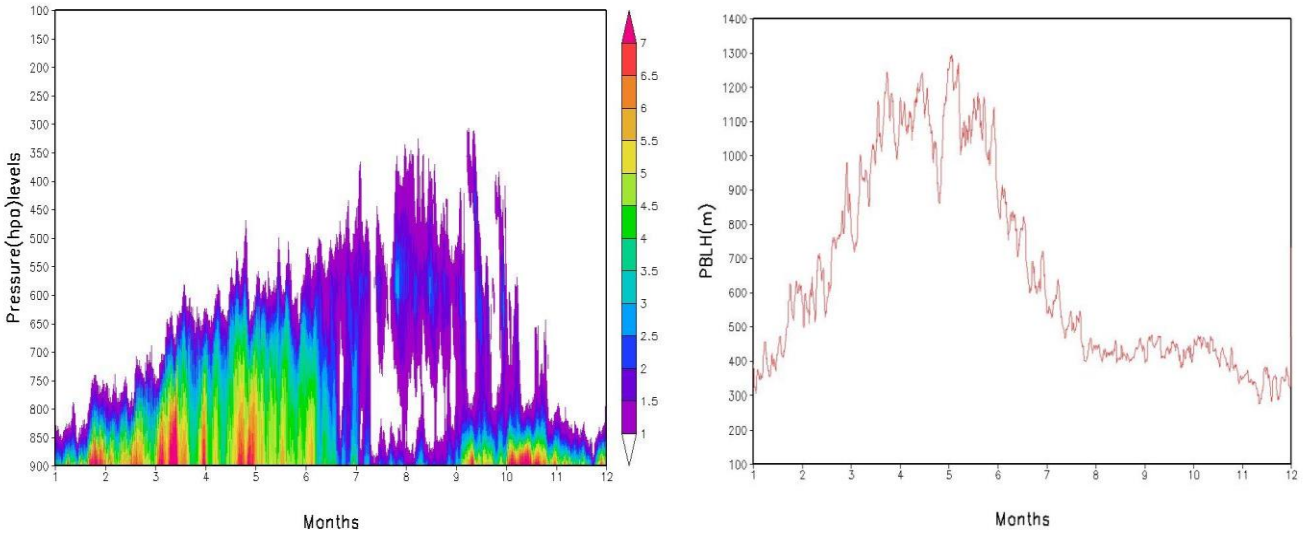

Figure 8

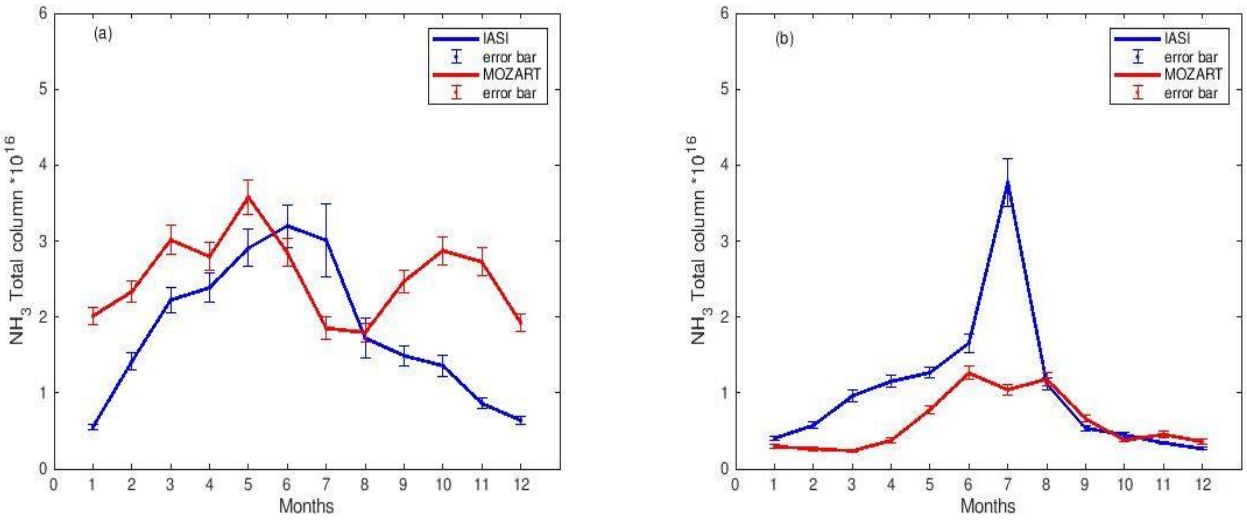
(a)
IASI
error bar
MOZART
error bar
NH_3 Total column *10^{16}
Months
(b)
IASI
error bar
MOZART
error bar
NH_3 Total column *10^{16}
Months

Figure 9

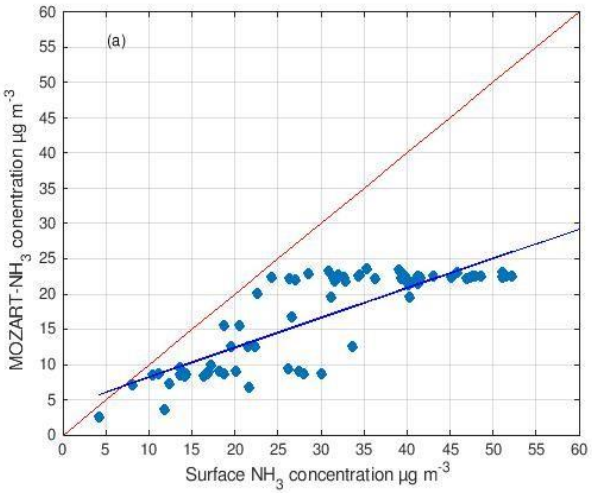
(a)
MOZART-NH3 conentration µg m-3
Surface NH3 concentration µg m-3

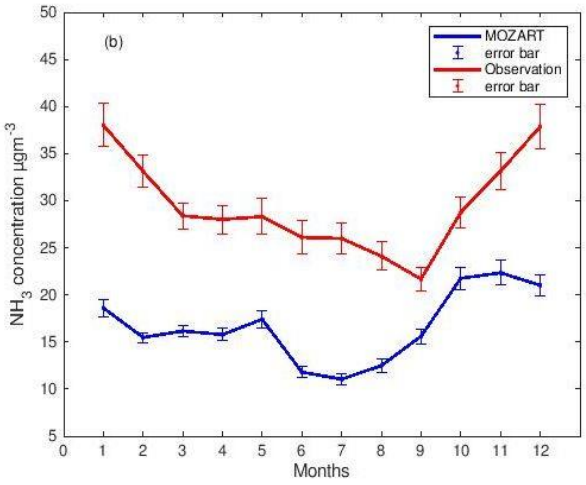
(b)
MOZART
error bar
Observation
error bar
NH3 concentration µgm-3
Months

Figure 10

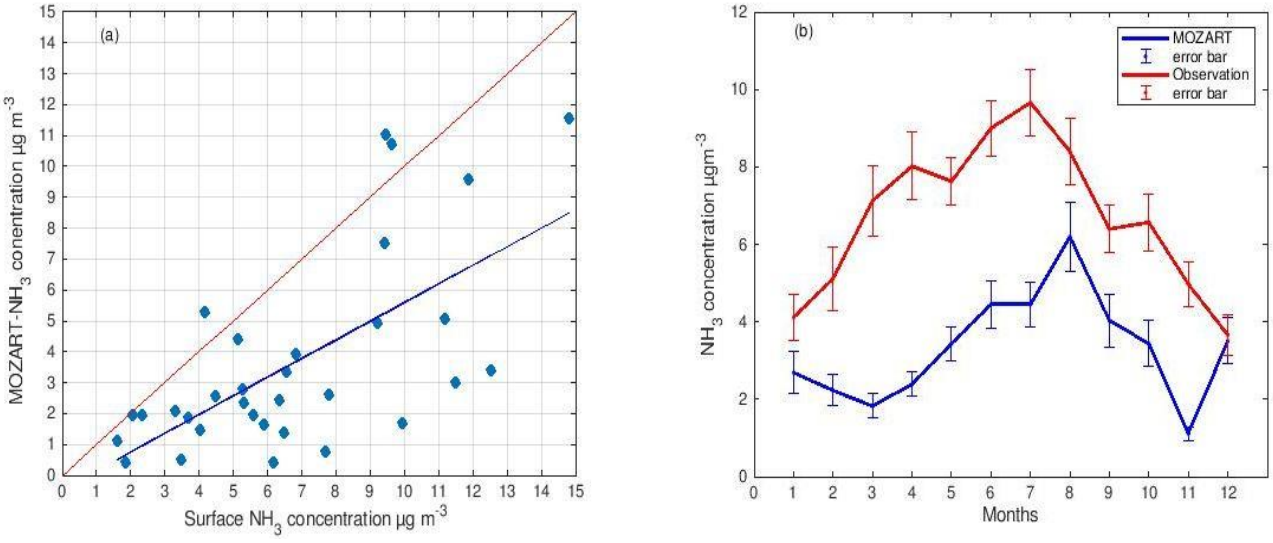
(a)
MOZART-NH3 conentration µg m-3
Surface NH3 concentration µg m-3
(b)
NH3 concentration µgm-3
Months
MOZART
error bar
Observation
error bar

Figure 11

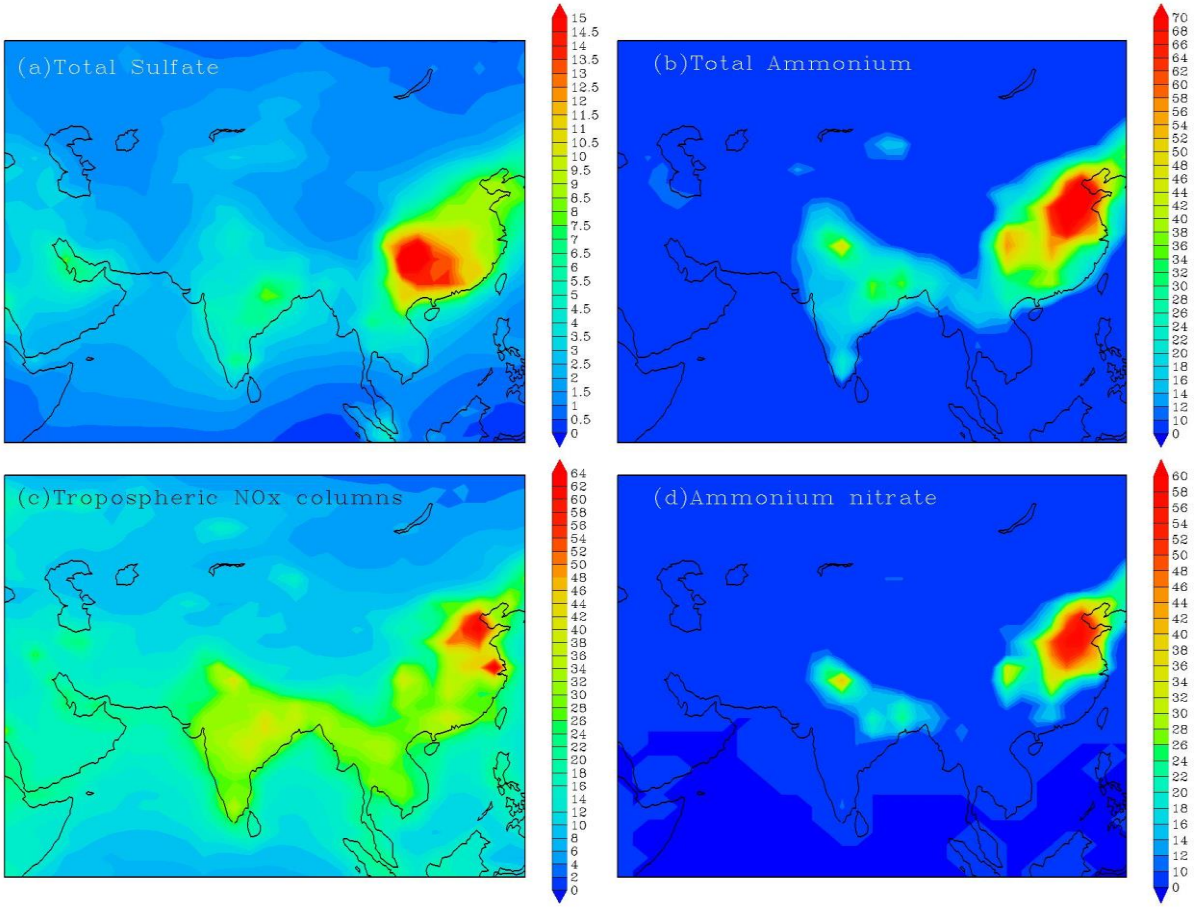

1185